The Arabidopsis m^{6}A-binding proteins ECT2 and ECT3 bind largely overlapping mRNA target sets and influence target mRNA abundance, not alternative polyadenylation

Laura Arribas-Hernández[1,5], Sarah Rennie[2], Michael Schon[3], Carlotta Porcelli[1], Balaji Enugutti[3], Robin Andersson[2], Michael Nodine[3,4], and Peter Brodersen[1,5,6]

[1]University of Copenhagen, Copenhagen Plant Science Center, Ole Maaløes Vej 5, DK-2200 Copenhagen N

[2] University of Copenhagen, Department of Biology, Ole Maaløes Vej 5, DK-2200 Copenhagen N

[3] Gregor Mendel Institute (GMI), Austrian Academy of Sciences, Vienna Biocenter (VBC), Dr. Bohr-Gasse 3, 1030 Vienna, Austria

[4] Laboratory of Molecular Biology, Wageningen University, Wageningen, 6708 PB, the Netherlands

[5] Corresponding author

[6] To whom requests for biological material should be addressed

Email LA-H: laura.arribas@bio.ku.dk; PB: pbrodersen@bio.ku.dk

Abstract

Gene regulation via *N6*-methyladenosine (m^6A) in mRNA involves RNA-binding proteins that recognize m^6A via a YT521-B homology (YTH) domain. The plant YTH domain proteins ECT2 and ECT3 act genetically redundantly in stimulating cell proliferation during organogenesis, but several fundamental questions regarding their mode of action remain unclear. Here, we use HyperTRIBE (targets of RNA-binding proteins identified by editing) to show that most ECT2 and ECT3 targets overlap, with only few examples of preferential targeting by either of the two proteins. HyperTRIBE in different mutant backgrounds also provides direct views of redundant and specific target interactions of the two proteins. We also show that contrary to conclusions of previous reports, ECT2 does not accumulate in the nucleus. Accordingly, inactivation of *ECT2*, *ECT3* and their surrogate *ECT4* does not change patterns of polyadenylation site choice in ECT2/3 target mRNAs, but does lead to lower steady state accumulation of target mRNAs. In addition, mRNA and microRNA expression profiles show indications of stress response activation in *ect2/ect3/ect4* mutants, likely via indirect effects. Thus, previous suggestions of control of alternative polyadenylation by ECT2 are not supported by evidence, and ECT2 and ECT3 act largely redundantly to regulate target mRNA, including its abundance, in the cytoplasm.

Introduction

N6-methyladenosine (m^6A) in mRNA is of fundamental importance in eukaryotic gene regulation (Zhao et al. 2017). Many functions of m^6A involve RNA binding proteins that recognize m^6A in mRNA via a YT521-B homology (YTH) domain (Stoilov et al. 2002; Dominissini et al. 2012; Wang et al. 2014; Zaccara et al. 2019). The YTH-domain family is subdivided into two phylogenetic groups, YTHDF and YTHDC (Patil et al. 2018; Balacco and Soller 2019), but the biochemistry used for m^6A recognition is identical in both groups: an aromatic cage provides a hydrophobic environment for the *N6*-methyl group and stacking interactions with the adenine ring (Li et al. 2014b; Luo and Tong 2014; Theler et al. 2014; Wang et al. 2014; Xu et al. 2014; Zhu et al. 2014), resulting in at least 10-fold higher affinity for m^6A-containing over non-methylated RNA. YTHDF proteins consist of an N-terminal intrinsically disordered region (IDR) followed by the YTH domain (Patil et al. 2018). Early reports seemed to indicate functional specialization of vertebrate YTHDF proteins for either translational activation or mRNA decay (Wang et al. 2014; Wang et al. 2015; Li et al. 2017; Shi et al. 2017), whereas recent studies support functional redundancy among the three YTHDFs in mammals and zebrafish (Kontur et al. 2020; Lasman et al. 2020; Zaccara and Jaffrey 2020), similar to the functional overlap described earlier for plant YTHDFs (Arribas-Hernández et al. 2018).

In plants, the YTHDF family is greatly expanded, with eleven members in *Arabidopsis*, referred to as EVOLUTIONARILY CONSERVED C-TERMINAL REGION1-11 (ECT1-11), compared to three in humans (Li et al. 2014a; Scutenaire et al. 2018). ECT2, ECT3 and ECT4 have important functions in post-embryonic development, but appear to work largely redundantly, at least in formal genetic terms. This is because single knockouts of *ECT2* or *ECT3* produce only subtle phenotypes related to branching patterns of epidermal hairs and root growth directionality, while simultaneous knockout of *ECT2* and *ECT3* results in delayed organogenesis and defective morphology of leaves, roots, stems, flowers, and fruits; defects that are exacerbated by additional mutation of *ECT4* in most cases (Arribas-Hernández et al. 2018; Arribas-Hernández et al. 2020). It remains unclear, however, which mRNAs are targeted by ECT2/3, and what the effects of ECT2/3 binding to them may be (Arribas-Hernández and Brodersen 2020). In particular, it is not clear whether the formal genetic redundancy between ECT2 and ECT3 is reflected in an overlapping target set, as would be expected for truly redundant action, or whether ECT2 and ECT3 might bind separate targets in wild type plants, but are able to replace each other in the artificial situation created by gene knockouts. The fact that knockouts of *ECT2* and *ECT3* have opposite effects on root growth directionality (Arribas-Hernández et al. 2020) clearly indicates that at least some level

of functional specialization exists between them, despite the obvious genetic redundancy observed in control of organogenesis. Thus, it is an open question of fundamental importance for understanding plant m^6A-YTHDF axes whether, and to what degree, mRNA targets of ECT2 and ECT3 overlap.

ECT2 has previously been suggested to act in the nucleus to influence alternative polyadenylation of targets (Wei et al. 2018). This model implies that plant ECT2 would act fundamentally differently from metazoan YTHDF proteins that are thought to be exclusively cytoplasmic and act to control mRNA fate via accelerated mRNA decay, or translational status (Patil et al. 2018; Zaccara et al. 2019), perhaps in some cases by influencing the ability of other RNA binding proteins to associate with specific mRNAs (Worpenberg et al. 2021). The evidence for nuclear localization of ECT2 is not unequivocal, however, because the ECT2 signal presumed to be nuclear has not been examined relative to a nuclear envelope marker. In contrast, all studies examining the subcellular localization of ECT2 (and ECT3 and ECT4) have clearly established their presence in the cytoplasm (Arribas-Hernández et al. 2018; Scutenaire et al. 2018; Wei et al. 2018; Arribas-Hernández et al. 2020). In addition, the model of ECT2-mediated gene regulation via alternative polyadenylation has not been tested by direct experimentation.

Here, we use the proximity-labeling method HyperTRIBE (targets of RNA binding proteins identified by editing) (McMahon et al. 2016; Xu et al. 2018) to identify mRNA targets of ECT3. HyperTRIBE uses fusion of an RNA-binding protein to a hyperactive mutant of the catalytic domain of the *Drosophila* adenosine deaminase acting on RNA (ADARcd) to obtain an A-G mutation profile specifically in mRNAs bound by the RNA-binding protein of interest *in vivo*. We combine comparative analysis of this dataset with the target identification of ECT2 by HyperTRIBE and iCLIP (individual nucleotide resolution crosslinking and immunoprecipitation) (König et al. 2010) reported in the accompanying paper, a series of transcriptomic analyses in *ect2/ect3/ect4* triple knockout mutants, and super-resolution microscopy of ECT2 localization, to establish three fundamental properties of mRNA regulation by ECT2 and ECT3. (1) Most targets are shared between ECT2 and ECT3, and the two proteins act genuinely redundantly *in vivo* to bind to and regulate many targets, in agreement with their similar expression patterns and genetically redundant functions (Arribas-Hernández et al. 2018; Arribas-Hernández et al. 2020). (2) ECT2/3/4 do not appreciably influence alternative polyadenylation of target mRNAs, consistent with the absence of ECT2-mCherry from the nucleoplasm. (3) In ECT2-expressing cell populations, the abundance of the majority of ECT2/ECT3-target mRNAs is reduced upon loss of ECT2/3/4 activity.

Results

Identification of ECT3 target mRNAs using HyperTRIBE

To identify target mRNAs of ECT3 transcriptome-wide, we chose HyperTRIBE, because of our demonstration in the accompanying paper that it efficiently identifies ECT2 targets with little expression bias. We therefore proceeded in exactly the same way as described for ECT2: among transgenic lines expressing *AtECT3pro:AtECT3-FLAG-DmADAR^{E488Q}cd-AtECT3ter* (henceforth "*ECT3-FLAG-ADAR*") in the triple *ect2-1/ect3-1/ect4-2* (*te234*) knockout background (Arribas-Hernández et al. 2018; Arribas-Hernández et al. 2020), lines with the highest degree of complementation were selected (*Figure 1A*) and used to define the level of ECT3-FLAG-ADAR protein required for *in vivo* function. Subsequently, we chose lines expressing similar levels of ECT3-FLAG-ADAR in *ect3-1* single mutants, and of FLAG-ADAR under the control of the *ECT3* promoter (henceforth simply "*FLAG-ADAR*") in wild type background to use as negative control (*Figure1—figure supplement 1A*). Five lines of each type were used for mRNA-seq of dissected shoot and root apices, and the data was analyzed to identify differentially edited sites (*Figure 1B, Figure1—figure supplements 1,2*). Despite the lower expression of *ECT3* compared to *ECT2* (Arribas-Hernández et al. 2018) and, consequently, generally lower editing proportions in *ECT3-FLAG-ADAR* lines compared to *ECT2-FLAG-ADAR* lines (*accompanying paper*) (*Figure 1C*), the implementation of the HyperTRIBE**R** pipeline to call significant editing sites successfully identified 2,448 targets in aerial tissues, and 3,493 in roots (ECT3 HT-targets) (*Figure 1B, Supplementary file 1*). As seen for ECT2 (*accompanying paper*), the ECT3 target genes in shoot and root apices largely overlapped, and the editing proportions of individual editing sites showed a strong correlation (*Figure 1D,E*). Accordingly, most aerial- or root-specific targets could be explained by differences in expression between tissues (*Figure 1F*). The identification of strongly overlapping target sets in roots and shoots is expected from the similar roles of ECT3 in promoting growth and cell division in the two tissues (Arribas-Hernández et al. 2020), and therefore, constitutes an argument for robustness of ECT3 target identification by the HyperTRIBE method

ECT2 and ECT3 bind to overlapping sets of targets

We next analyzed the degree to which ECT2 and ECT3 HT-targets overlap. The datasets are directly comparable, as growth conditions, tissue dissection, RNA extraction, library construction and sequencing depth for target identification of ECT3 by HyperTRIBE were identical to those used for ECT2 (*accompanying paper*) (*Figure 2—figure supplement 1*). Remarkably, more than 94% of ECT3 HT-targets overlapped with the larger group of ECT2 HT-targets in both aerial and root

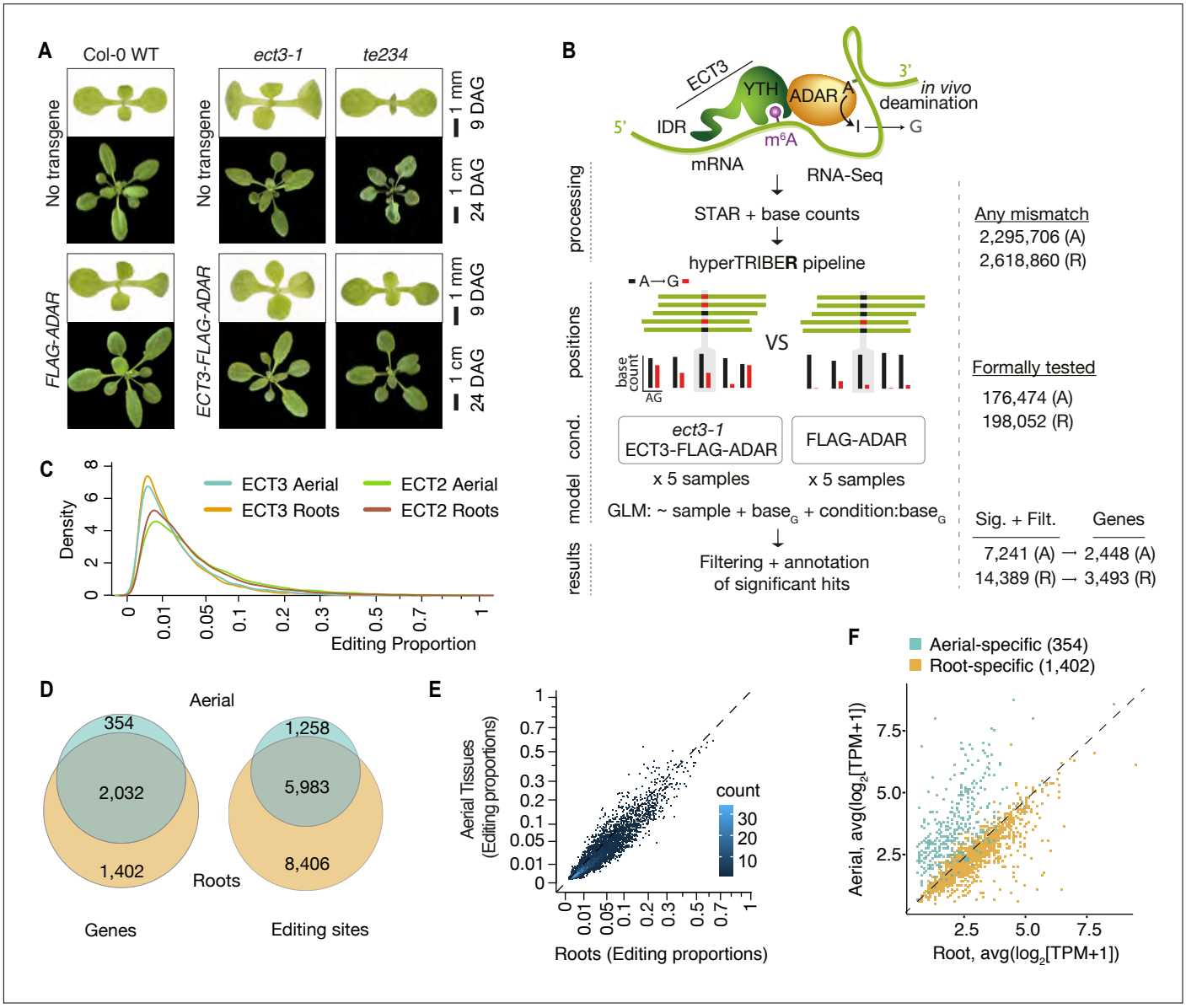

Figure 1. Identification of ECT3 targets using HyperTRIBE. (A) Phenotypes of wild type, *ect3-1* and *te234* (*ect2-1/ect3-1/ect4-2*) mutants with (lower panels) or without (upper panels) *ECT3pro:ECT3-FLAG-DmADAR^{E488Q}cd-ECT3ter* (*ECT3-FLAG-ADAR*) or *ECT3pro:FLAG-DmADAR^{E488Q}cd-ECT3ter* (*FLAG-ADAR*) transgenes, at 9 or 24 days after germination (DAG). **(B)** Experimental design for ECT3-HyperTRIBE (ECT3-HT) target identification. After quantifying nucleotide base counts from mapped RNA-seq libraries of *ect3-1 ECT3-FLAG-ADAR* and *FLAG-ADAR* lines, all positions with mismatches were passed into the HyperTRIBE**R** pipeline to call significant editing sites. Identified sites were further filtered to remove SNPs and retain only A-to-G mismatches. The number of sites in either aerial (A, dissected apices) or root (R, root tips) tissues at each stage is indicated. GLM, generalized linear model. **(C)** Density of editing proportions for significant editing sites in aerial tissues and roots of *ect3-1/ECT3-FLAG-ADAR* and *ect2-1/ECT2-FLAG-ADAR* (*accompanying manuscript*) lines. **(D)** Overlap between ECT3-HT target genes and editing sites in roots and aerial tissues, out of the set of genes commonly expressed in both tissues. **(E)** Scatterplot of the editing proportions of significant editing sites in ECT3-HT for aerial vs root tissues. **(G)** Scatterplot showing the expression in aerial and root tissues (mean $\log_2$(TPM+1) over the 5 ECT3-HT control samples) of the genes that are identified as targets only in aerial tissues or only in roots.

Figure supplement 1. Identification of ECT3 targets using HyperTRIBE (extended data).

Figure supplement 2. Characteristics of ECT3-HyperTRIBE editing sites relative to target expression levels.

tissues, and there was a clear correlation between the editing proportions of the common editing sites, albeit with higher editing by ECT2-FLAG-ADAR overall (*Figure 2A,B*). Indeed, the pattern of editing sites resulting from fusion of ADAR to ECT2 or ECT3 was similar for many targets, with a few more sites typically detected in the ECT2-HT dataset (e.g. *ATP-Q*, *Figure 2C left panel*). Nevertheless, we also noticed examples with preferential targeting by ECT2-FLAG-ADAR (e.g. *TUA4*, *Figure 2C middle panel*) or, interestingly, by the less abundant ECT3-FLAG-ADAR (e.g. *UBQ6*, *Figure 2C right panel*), perhaps hinting to molecular explanations for the recently described non-redundant roles of ECT2 and ECT3 in determining root growth directionality (Arribas-Hernández et al. 2020). Overall, however, the overwhelming overlap between ECT2 and ECT3 HT-targets in both tissues suggests that binding to the same mRNA targets underlies their genetically redundant functions in leaf and root formation (Arribas-Hernández et al. 2018; Arribas-Hernández et al. 2020). We also observed that *ECT2* and *ECT3* mRNAs contain m^6A sites in seedlings according to published datasets (Shen et al. 2016; Parker et al. 2020), and that their protein products target their own and each other's transcripts (*Figure 2—figure supplement 2*), indicating that autoregulatory feedback may contribute to control their expression.

HyperTRIBE provides direct views of redundant target mRNA interactions with ECT2 and ECT3

Although the demonstration that ECT2 and ECT3 bind to strongly overlapping target sets is consistent with largely redundant *in vivo* function, it does not constitute a direct proof. For example, the proteins may bind to the same targets, but in different cells such they act *de facto* non-redundantly. We reasoned that HyperTRIBE might provide a means to observe directly whether ECT2 and ECT3 act specifically or redundantly on shared targets, and whether one ECT protein acquires non-natural targets upon knockout of the other by comparison of editing proportions measured with ADAR fusions expressed in single vs. triple mutant backgrounds. The single mutant background (e.g. *ECT2-FLAG-ADAR* in *ect2-1*) would mimic the wild type setting, while the triple mutant background (e.g. *ECT2-FLAG-ADAR* in *te234*) would probe target interactions in the absence of redundant or competing proteins, but still in plants with wild type growth rates (*Figure 1A; accompanying paper*). Redundant target interactions would be expected to result in generally higher editing proportions of the same targets as those identified in single mutant backgrounds, especially for the least expressed protein, ECT3 (*Figure 3—figure supplement 1*). Conversely, specific interactions would cause one of two possible signatures. (i) In the case of cell-type specific interactions, no change in editing proportions between single and triple mutant backgrounds should

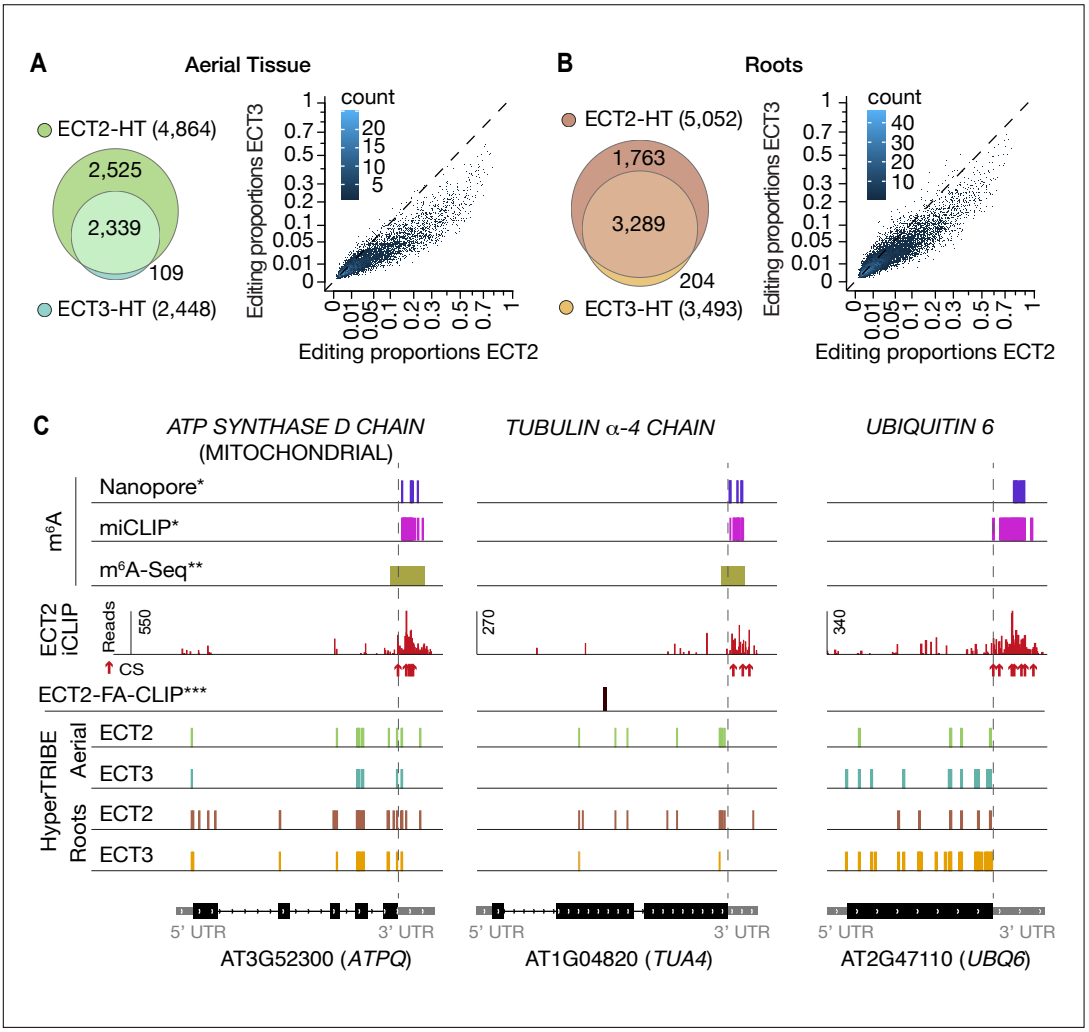

Figure 2. ECT3 targets are fewer and largely contained within ECT2 targets. (A, B) Left panels: overlap of ECT2-HT and ECT3-HT targets, for the set of commonly expressed genes, in aerial (A) and root (B) tissues. Right panels: Scatter plots showing the editing proportions of editing sites between ECT2-HT and ECT3-HT, for all significant positions common to both sets, separately for aerial tissues (A) and roots (B). **(C)** Examples of common ECT2 and ECT3 targets showing the distribution of ECT2/3-HT editing sites sites in either roots or shoots along the transcript. The distribution of ECT2-iCLIP reads and peaks, FA-CLIP peaks***, and m^{6}A sites*,** is also shown. * Parker et al. (2020); ** Shen et al. (2016); *** Wei et al. (2018).

Figure supplement 1. Sequencing depth of ECT2 and ECT3 HyperTRIBE RNA-seq data.

Figure supplement 2. ECT2 and ECT3 target each other and themselves.

be detectable. (ii) In the case of specific interactions within the same cells in wild type, but non-natural targeting in the absence of other ECT proteins, acquisition of non-natural targets in triple mutant backgrounds is expected. We observed widespread increases in editing proportions for ECT3 targets upon removal or ECT2/4, while such increases occurred only sporadically for ECT2 targets (*Figure 3A-C, Supplementary file 2*), supporting the idea of largely redundant target interactions. Furthermore, although more sites showed increased editing by ECT3-FLAG-ADAR in aerial tissues than in roots in the absence of ECT2/4 (*Figure 3B*), the net increase of editing proportions was higher in roots for both ECT2 and ECT3 (*Figure 3C*), consistent with the more dominant role of ECT2 over ECT3 in aerial tissues compared to roots (*Figure 2A,B*). Importantly, the higher editing proportions in the triple mutant background cannot be trivially explained by higher expression of the transgene in these lines, as the average expression was comparable or slightly lower (*Figure 3—figure supplement 1*). These observations directly support genuinely redundant interactions of ECT2 and ECT3 with the majority of their mRNA targets *in vivo*.

Small sets of specific ECT targets acquire unnatural ECT interactions in knockout backgrounds

Although the tendency of ECT2/3 to show redundant target mRNA interactions was widespread, we also looked for examples of specific interactions in the HyperTRIBE data in single and triple mutants. A priori, we considered targets to be ECT2-specific if they were detected by ECT2-FLAG-ADAR, but not ECT3-FLAG-ADAR, in single mutant backgrounds (strictly specific), or became edited by ECT3-FLAG-ADAR only in the triple mutant background. The definition of ECT3-specific targets followed analogous criteria. However, because ECT2 expression is much higher than ECT3 expression (*Figure 3—figure supplement 1*), ECT2-specific targets identified in this way may simply be below the detection limit of the less highly expressed ECT3-FLAG-ADAR transgene. Hence, arguments for existence of *bona fide* specific targets must take detectability by ECT3-FLAG-ADAR into account. Consistent with expectation from the different ECT2/ECT3 dosage, much larger numbers of strictly ECT2-specific transcripts were identified compared to ECT3: 2,414 ECT2-specific and 93 ECT3-specific targets were identified in aerial tissues, while in roots, 1,738 were ECT2-specific and 197 were ECT3-specific (*Figure 3D,E, Figure 3—figure supplement 2*). In addition, small sets of specific target mRNAs became targets of the other ECT protein upon knockout of its genuine interacting protein (110 and 24 for ECT2-specific targets in aerial and root tissues respectively, and 2 for ECT3-specific targets in roots) (*Figure 3D,E, Figure 3—figure supplement 2*). These sets constitute outstanding candidates for ECT2/3-specific mRNA targets.

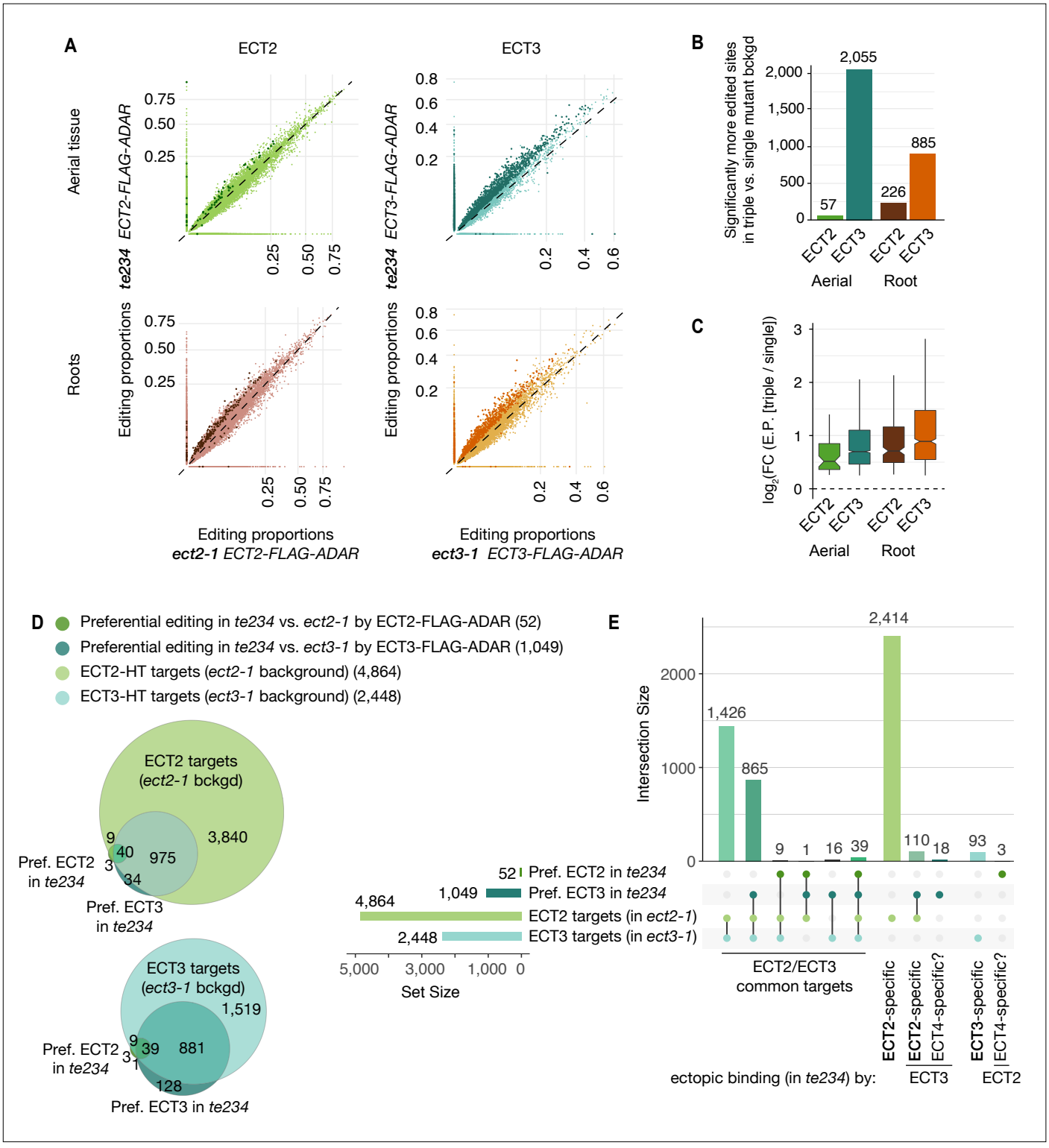

Figure 3. Redundancy between ECT2 and ECT3. (A) Scatterplots comparing the editing proportions of ECT2- and ECT3-FLAG-ADAR observed in triple vs. single mutant backgrounds in aerial and root tissues. They include all positions significantly edited with respect to FLAG-ADAR controls (p-value < 0.01, $\log_2$(FC)>1) in either background, with dots on the axes reflecting positions not significantly edited in one of the two backgrounds. Dots in darker shades indicate positions more highly edited in one background compared to the other (p-value < 0.1, log2(FC)>0.25 or log2(FC)<-0.25). **(B)** Barplots showing the number of positions significantly more edited in triple vs. single mutant background for each tissue and ECT protein. Positions significantly less edited in triple mutant background were less than 12 in all cases. **(C)** Boxplots showing fold changes in editing proportions between triple and single mutant background for the 2 ECT proteins and tissues studied. **(D,E)** Venn diagrams (D) and Upset plot (E) showing the overlap between the ECT2 and ECT3-HT target sets (in single mutant backgrounds) with the groups of genes with more highly edited positions in the triple mutant background in aerial tissues (the equivalent for roots is shown in *Figure3—figure supplement 2*).

Figure supplement 1. Expression levels (TPM) of the FLAG-ADAR-containing transgenes in all HyperTRIBE lines.

Figure supplement 2. Overlap between ECT2/3-HT targets in single and triple mutant background in roots.

Curiously, a few transcripts (21 in aerial tissues and 9 in roots) were edited by either ECT2 or ECT3 only in the triple mutant background (*Figure 3D,E, Figure 3—figure supplement 2*). Because *ECT4* is also knocked out in *te234*, these sets define putative ECT4-specific targets. In summary, our comparative analyses of ECT2/3 HyperTRIBE data obtained in single and triple mutant backgrounds indicate that redundant target interaction is pervasive, but they also identify small target sets with properties consistent with preferential interaction with only one ECT protein.

ECT2/3 targets tend to be co-expressed in proliferating cells and are enriched in functions related to basic metabolism and protein synthesis

We next combined the ECT3-HT target set described here with the ECT2 iCLIP and ECT2-HT data (*accompanying manuscript*) to define three gene sets of particular interest for functional analysis of ECT2/3: **The permissive target set** (6,528 genes) defined as genes with either ECT2 HT, ECT3 HT or ECT2 iCLIP support, the **stringent target set (**1,992 genes) defined as all ECT2 or ECT3 HT-targets that are also in the ECT2 iCLIP target set, and **the non-target set** (13,504 genes) defined as all expressed genes not contained in the permissive target set (*Figure 4A*, *Figure 4—figure supplement 1, Supplementary file 3*). As an initial check of consistency of the target sets with the biological context in which ECT2 and ECT3 function, we used single-cell transcriptome analysis of Arabidopsis roots (Denyer et al. 2019; Ma et al. 2020) to analyze the overlap of ECT2/3 expression with the enrichment of markers for different cell types in the permissive target set. This analysis showed reassuring congruence between predominant expression of ECT2/3 in meristem clusters and marker enrichment for these same clusters among targets (*Figure 4B, Figure 4—figure supplement 2*). We also analyzed the permissive target sets for groups of functionally related genes, and found that ECT2/3 targets are enriched in housekeeping genes, many related to basic metabolism and protein synthesis (*Figure 4C*). These initial analyses provide well-defined common ECT2/ECT3 target sets for further functional analysis.

Recovery of ECT2-expressing cell populations with and without ECT2/ECT3/ECT4 activity

ECT2, *ECT3* and *ECT4* expression is largely restricted to rapidly dividing cells of organ primordia (Arribas-Hernández et al. 2018; Arribas-Hernández et al. 2020), and since many ECT2/3 targets are broadly expressed housekeeping genes (*Figure 4C*), cell populations expressing ECT2-4 need to be isolated prior to transcriptome analyses to avoid confounding effects from cells that do not express these m^6A readers. We therefore used the fact that *ect2-1*/*ECT2-mCherry* exhibits root growth rates similar to wild type while *te234*/*ECT2*^{W464A}*-mCherry* exhibits clearly reduced root

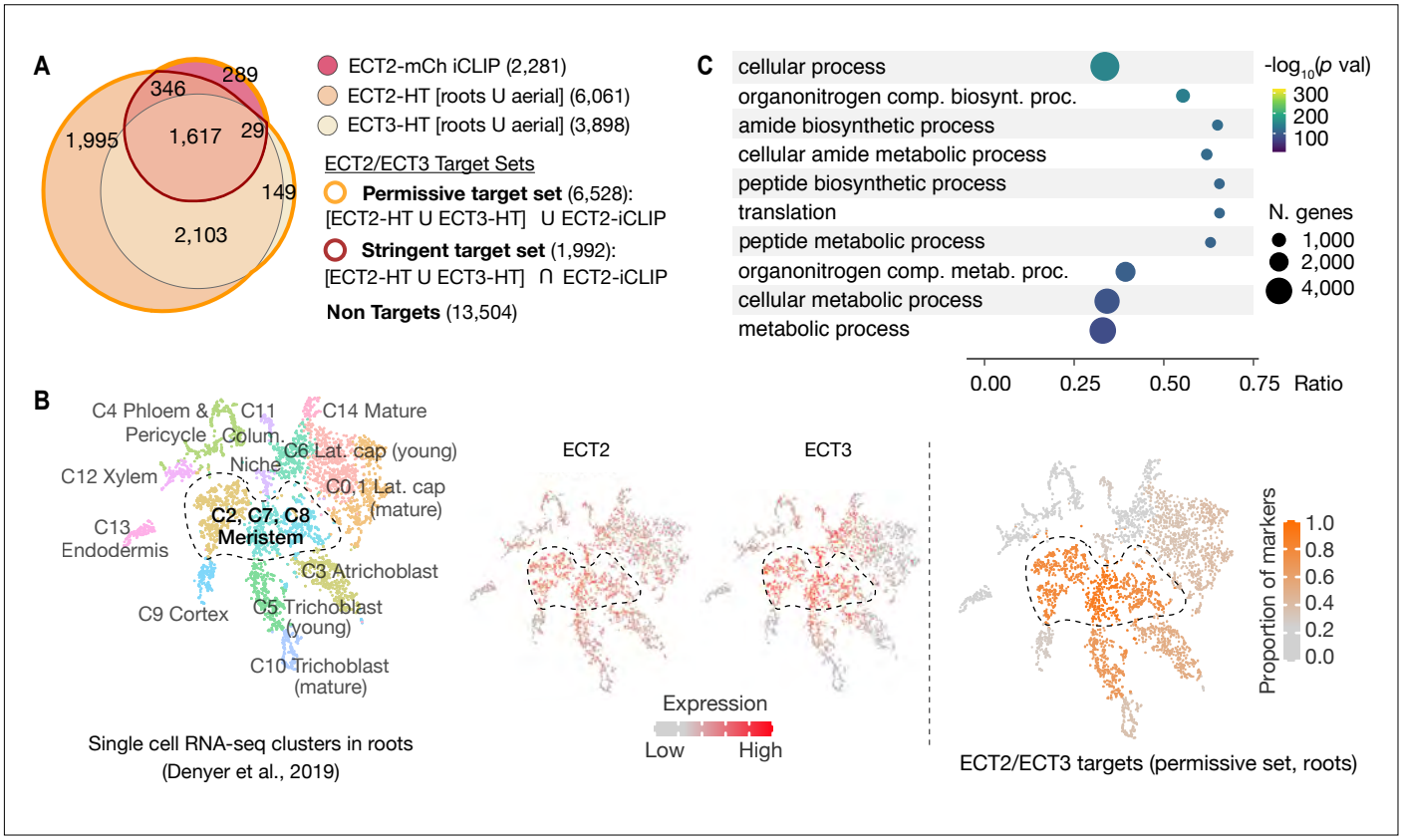

Figure 4. ECT2 and ECT3 targets are co-expressed with ECT2 and 3 in proliferating cells and enriched in biosynthetic processes. (A) Overlap between ECT2-iCLIP target genes with ECT2-HT and ECT3-HT target gene sets. Regions outlined in bold orange and red indicate the defined permissive and stringent ECT2/3 target sets in whole seedlings, respectively (aerial and root-specific target sets are shown in the figure supplement 1). Non-targets are all expressed genes (with detectable transcript levels in the corresponding HyperTRIBE RNA-Seq datasets) that are not in the permissive target set. **(B)** Left: t-SNE plot for scRNA-seq data in roots from Denyer et al. (2019), with cells colored according to their cell-type cluster definitions (see figure supplement 2 for details). Center: ECT2 and ECT3 single cell expression levels overlayed on to the t-SNE plot (Ma et al., 2020). Right: t-SNE plot with cell-type clusters shaded according to the proportion of marker genes from Denyer et al. (2019) that are targets of ECT2 or ECT3 in roots. Dashed enclosed region indicates clusters that contain meristematic cells. **(C)** The 10 most significantly enriched GO terms among ECT2/3 targets (permissive set).

Figure supplement 1. ECT2 and ECT3 target sets in aerial and root tissues.

Figure supplement 2. ECT2/ECT3 targets are co-expressed with *ECT2/3* in highly dividing root cells

growth rates nearly identical to *te234* triple knockouts (Arribas-Hernández et al. 2020), and applied fluorescence-associated cell sorting to select mCherry-expressing cell populations from root protoplasts of three independent transgenic lines for each of these two genetic backgrounds (*Figure 5A*). Because wild type and mutant fluorescent proteins have the same expression level, pattern, and intracellular localization (*Figure 5B,C*), this procedure yielded comparable ECT2-expressing cell populations (*Figure 5D, Figure 5—figure supplement 1*) with (*ECT2-mCherry/ect2-1/ECT3/ECT4*, henceforth "wild type") or without (*ECT2^{W464A}-mCherry/ect2-1/ect3-1/ect4-2,* henceforth "mutant") ECT2/3/4 function. We therefore isolated mRNA and constructed Smart-Seq2 libraries for comparison of location of poly(A) sites (PASs) and abundance of ECT2/3 targets and non-targets in *ECT2*-expressing cells from plants of the two different genetic backgrounds. Compared to standard mRNA-seq, Smart-seq2 recovers more reads with untemplated As (beginning of poly(A) tails) in addition to gene-specific sequence and can, therefore, be used for PAS mapping. We note that the selection of ECT2-expressing cells from the root meristem division zones of wild type and mutant lines also circumvents the trouble of preparing comparable samples from intact tissues of plants at different developmental stages despite having the same age.

ECT2/3/4 do not play a direct role in alternative polyadenylation of targets

We first addressed the conjecture on a nuclear role of ECT2 in PAS selection (Wei et al. 2018). In plants, PASs are not sharply defined but rather spread along localized regions and can be grouped into PAS clusters (PACs) for analysis (Wu et al. 2011; Sherstnev et al. 2012). Using a modification of the nanoPARE analysis pipeline (Schon et al. 2018) to map PASs from reads with ≥ 9 untemplated As, we identified a total of 14,667 PACs belonging to 12,662 genes after filtering possible false positives (*Methods*, *Figure 5—figure supplement 2A,B, Supplementary file 4*). We found no tendency for ECT2/3 target mRNAs to have more PACs than non-targeted genes (*Figure 5—figure supplement 2C*), suggesting that differential PAC location in ECT2/3 targets between mutant and wild type is not prevalent. Nevertheless, we specifically tested whether PASs could be affected by the loss of ECT2/3/4 function in two different ways: either a shift of the dominant PAC to an alternative PAC altogether, or a shift in the most common PAS within clusters. Sorting the 206 genes for which the dominant PAC differed between wild type and mutant samples (18.5% of the 1,114 genes with more than one PAC) into the ECT2/3 target groups in roots (*Figure 4—figure supplement 1B, Supplementary file 4*) showed that both the permissive and stringent targets were significantly less likely than non-targets to have a different dominant PAC upon loss of ECT2/3/4 function (p=0.013 and p=1.21e-5 for strictly permissive and stringent targets respectively; Fisher's

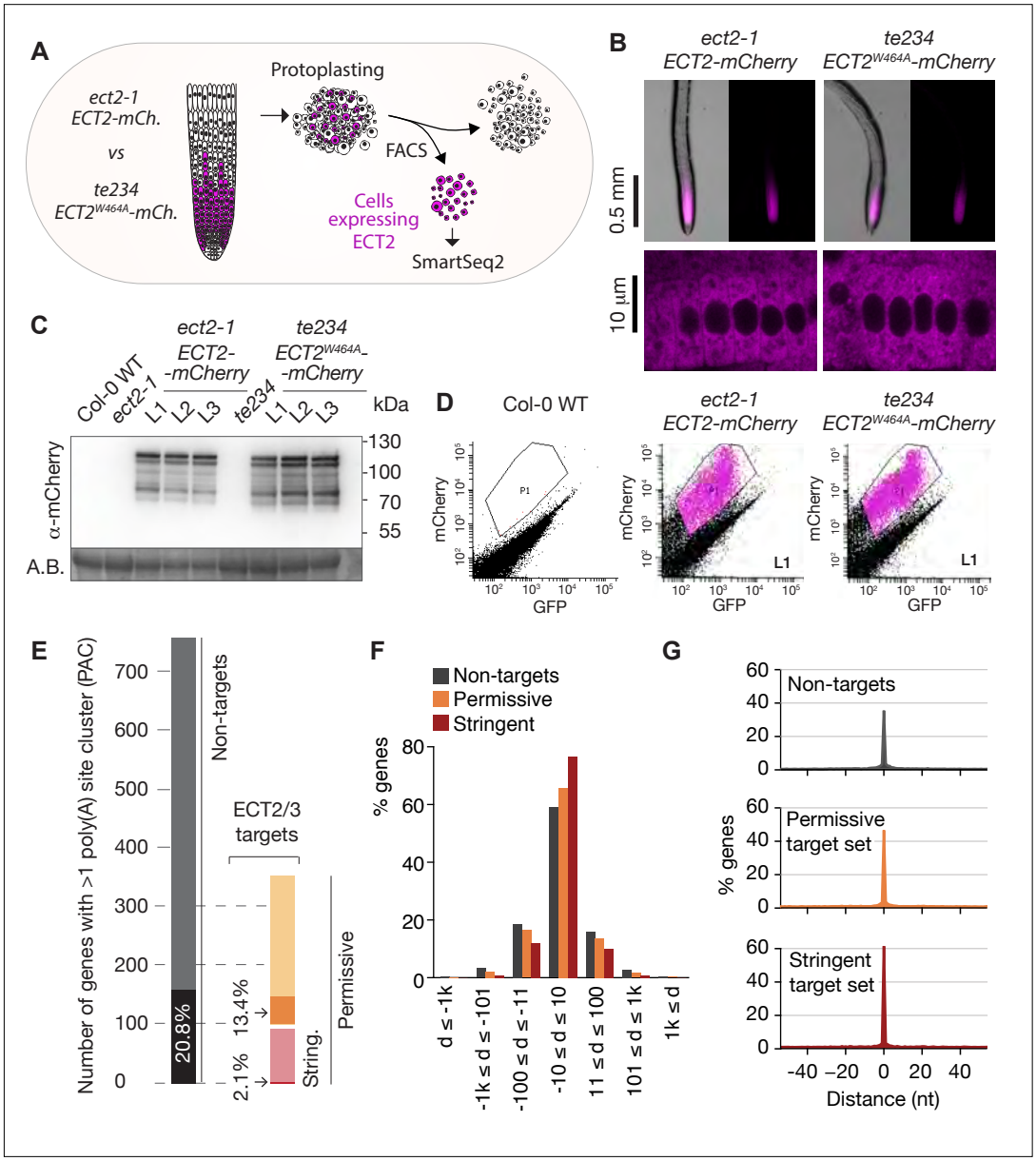

Figure 5. Poly(A) sites in ECT2/3 targets do not change upon loss of ECT2/3/4 function. (A) Experimental design. The experiment was performed once, using 3 biological replicates (independent lines) per group (genotype). **(B)** Expression pattern of ECT2-mCherry in root tips of *ect2-1 ECT2-mCherry* and *te234 ECT2^{W464A}-mCherry* genotypes by fluorescence microscopy. **(C)** Protein blot showing expression levels of ECT2-mCherry in the 3+3 lines of *ect2-1 ECT2-mCherry* and *te234 ECT2^{W464A}-mCherry* used as biological replicates for FACS selection of ECT2-expressing cells. Amido black (A.B.) is used as loading control. **(D)** Fluorescence profile (mCherry vs. GFP fluorescence) of root cells (protoplasts) from the transgenic lines in C. The complete set of lines/samples is shown in the figure supplement 1. Non-transgenic Col-0 WT is shown as control for background autofluorescence. Cells with a fluorescence profile within the outlined areas were selected for RNA extraction, Smart-seq2 library construction and sequencing. **(E)** Genes with more than one polyA site cluster (PAC) in the different target/non-target sets. Dark shades are genes in which the dominant PAC in *te234 ECT2^{W464A}-mCherry* samples differs from the one in *ect2-1 ECT2-mCherry*. **(F,G)** Distribution of distances (d [nt]) of the most common poly(A) site between *te234 ECT2^{W464A}-mCherry* and *ect2-1 ECT2-mCherry* samples for all genes where the most common poly(A) site could be determined in both genotypes (6,648 non-targets, 4,072 permissive targets, and 1,486 stringent targets). Negative values are upstream (5') and positive values are downstream (3') relative to the gene orientation. (F) Distances are binned by ±10, ±100, ±1000, and >1,000bp. (G) Distances are plotted by nucleotide in a ±40bp window.

Source data 1-3. Uncropped labelled panels and raw image files - *Figure 5C*.

Figure supplement 1. FACS-sorting of root protoplasts expressing ECT2-mCherry.

Figure supplement 2. Poly(A) sites do not change in ECT2/3 targets upon loss of ECT2/3/4 function (extended data).

exact test) (*Figure 5E, Figure 5—figure supplement 2C,D*). This significant depletion may be an effect of the higher expression of targets compared to non-targets (*accompanying manuscript*), as accuracy of PAS detection increases with transcript abundance (see *Figure 5—figure supplement 2E* for details). The result indicates that the alternative polyadenylation observed upon loss of ECT2/3/4 function is not prevalent among ECT2/3 targets. Finally, we examined changes to the local distribution of PASs within clusters. We defined the most common PAS as the single position in all overlapping PACs with the most reads, and determined the distance between such dominant PASs in wild type and mutant samples. Comparison of the distances revealed that the most common PAS does not change by more than 10 bp in the majority of genes, and is not more likely to be different in ECT2/3 targets than in non-targets (*Figure 5F*). In fact, the most common PAS is more likely to be unchanged in targets than in non-targets (*Figure 5G*) (p=0.028 and p=2.2e-16 for strictly permissive and stringent targets respectively; Fisher's exact test). Taken together, these analyses show that neither the usage of alternative PACs nor the dominant PASs within clusters have any tendency to change in ECT2/3-targets upon loss of ECT2/3/4 function.

ECT2-mCherry does not localize to the nucleoplasmic side of the nuclear envelope

To further investigate whether ECT2 may have any nuclear functions, we revisited the evidence for localization of ECT2 in the nucleoplasm, which is based on confocal fluorescence microscopy of ECT2-GFP or YFP-ECT2 in DAPI-stained root cells of stable Arabidopsis lines (Scutenaire et al. 2018; Wei et al. 2018). Because (i) the localization of ECT2-mCherry in living root cells of our lines has a general sharp boundary with what we interpreted to be the nucleus (*Figure 5B*) (Arribas-Hernández et al. 2018) and does not overlap with nucleoplasmic MTA-TFP (Arribas-Hernández et al. 2020), (ii) paraformaldehyde fixation routinely used to permeate DAPI inside plant tissues (used by Scutenaire et al. and not specified by Wei et al.) can introduce artifacts in the localization of fluorescent proteins (Li et al. 2015), and (iii) the RNA-binding properties of DAPI could yield signal from the RNA-rich rough endoplasmic reticulum surrounding the nucleus (Tanious et al. 1992), we decided to examine the localization of ECT2-mCherry relative to the nuclear envelope in living cells. We therefore crossed lines expressing functional ECT2-mCherry (Arribas-Hernández et al. 2020) with plants expressing the outer nuclear envelope and nuclear pore complex-associated protein WIP1 fused to GFP (Xu et al. 2007). Confocal fluorescence microscopy of intact roots showed that the sharp boundaries of the ECT2-mCherry expression domain were delimited by the GFP-WIP1 signal from the nuclear envelope (*Figure 6A, Figure 6—figure supplement 1A*). Importantly, the occasional points at which the ECT2-mCherry signal seemed to fuzzily spill into the nucleus (white arrows in *Figure 6A, Figure 6—figure supplement 1A*) overlapped with equally blurry GFP-WIP1

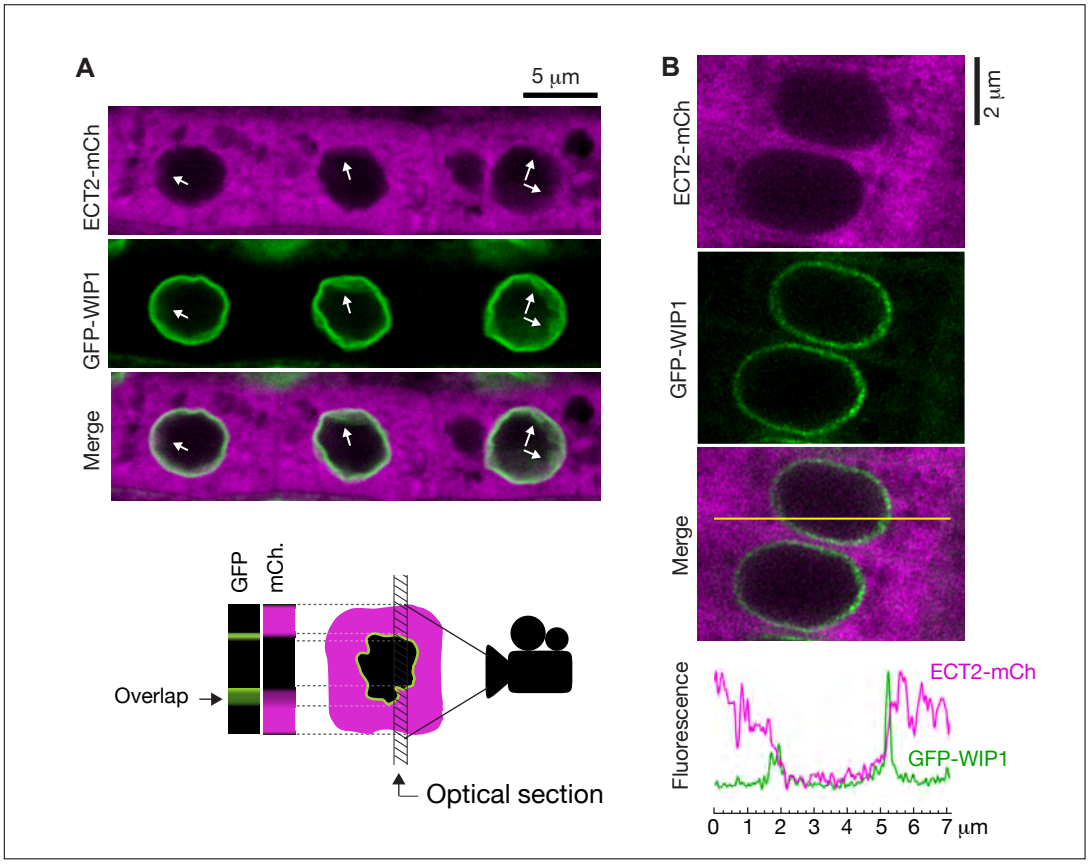

Figure 6. ECT2 is not in the nucleus. (**A**) Standard confocal microscopy of root cells co-expressing *ECT2-mCherry* and *GFP-WIP1*. White arrows indicate areas in which apparent spills of ECT2-mCherry signal into the nucleus overlap with blurry GFP signal from the nuclear envelope, a sign of not-perpendicularity between the envelope and the optical plane as exemplified on the cartoon at the bottom. (**B)** Airyscan super-resolution confocal microscopy of root cells as in A. The image is cropped from a larger picture shown in the figure supplement 1. mCherry and GFP fluorescence signals along the yellow line show absence of ECT2-mCherry inside the limits of the GFP-labelled nuclear envelope.

Figure supplement 1. Super-resolution confocal microscopy of cells co-expressing ECT2-mCherry and the nuclear envelope marker GFP-WIP1.

signal, probably due to lack of perpendicularity between the nuclear envelope and the optical section in these areas. In such cases, the cytoplasm, nucleus and nuclear envelope may be contained in the same region of the optical section and thus appear to be overlapping (*Figure 6A, bottom panel*). To verify this interpretation, we inspected our plants with the super-resolution confocal Airyscan detector (Huff 2015) and, as expected, we did not observe ECT2-mCherry signal inside the GFP-WIP1-delimited nuclei in any instances (*Figure 6B, Figure 6—figure supplement 1B,C*). Based on these analyses, we conclude that ECT2 resides in the cytoplasm and its presence in the nucleus, if any, may be too transient to be detected by fluorescence microscopy. These results agree with the lack of evidence for a function of ECT2/3/4 in choice of PAS, and strongly suggest that the molecular basis for the importance of ECT2/3/4 should be sought in cytoplasmic properties of their mRNA targets.

ECT2/3 targets tend to show reduced abundance upon loss of ECT2/3/4

We next assessed the effect of loss of ECT2/3/4 function on target mRNA abundance, using the Smart-seq2 data from FACS-sorted root protoplasts described above. Principal component analysis showed that the three repeats of wild type (*ect2-1/ECT2-mCherry*) were well separated from the three repeats of mutant (*te234/ECT2^{W464A}-mCherry*) along the first principal component (*Figure 7—figure supplement 1A*), indicating that differential gene expression analysis with mutant to wild type comparison was meaningful. We focused on stringent, permissive and non-ECT2/3 targets in roots (*Figure 4—figure supplement 1B, Supplementary file 3*), and visualized their differential expression between mutant and wild type by scatter, volcano and box plots (*Figure 7A-C, Supplementary file 5*). These approaches showed that stringent targets have a clear tendency towards down-regulation upon loss of ECT2/3/4 function. This trend is maintained, but is less pronounced in permissive targets, and is reversed in non-targets (*Figure 7A-C*). Indeed, of the significantly differentially expressed stringent ECT2/3 targets, nearly all were down-regulated in the mutant, while the majority of differentially expressed non-targets were up-regulated compared to wild type (*Figure 7D*). Furthermore, ECT2/3 targets accounted for more than half of all significantly downregulated genes, but only about 15% of upregulated genes (*Figure 7E*). In contrast, highly upregulated genes tended to be non-targets (*Figure 7B, right panel*).

Functional groups of differentially expressed genes

To test if these differentially regulated gene sets represented subsets of functionally related genes within target and non-target groups, we analyzed their potential enrichment of GO terms. This

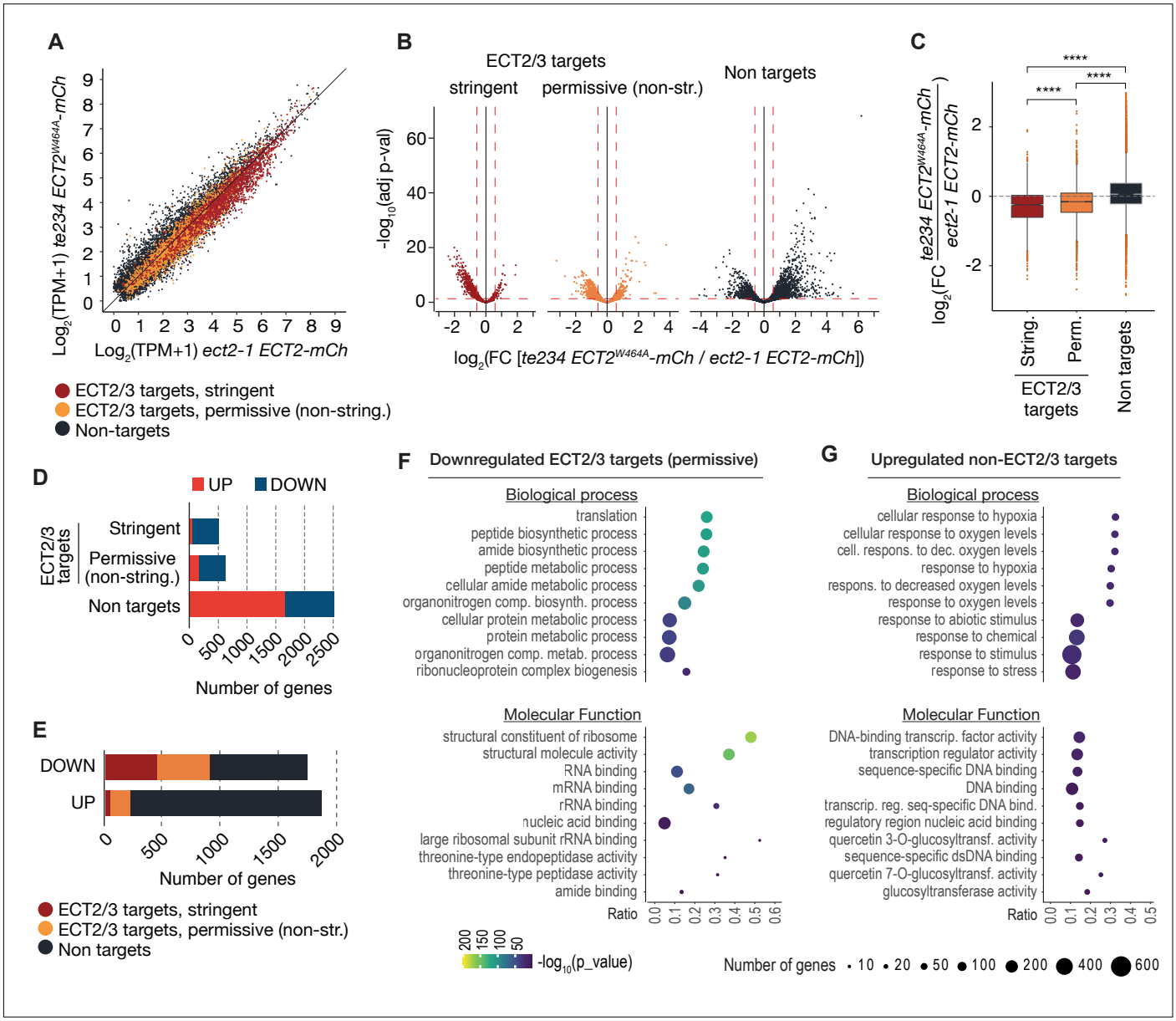

Figure 7. ECT2/3 targets are generally less abundant in cells without ECT2/3/4 function. (A) Scatterplot of TPM expression values in Smart-seq2 libraries of root protoplasts expressing ECT2-mCherry in *te234/ECT2^{W464A}-mCherry* vs. *ect2-1/ECT2-mCh* samples. **(B)** Volcano plots reveal genes differentially expressed between the genotypes described in A. **(C)** Boxplots of $\log_2$ fold change expression values between *te234/ECT2^{W464A}-mCherry* and *ect2-1/ECT2-mCh samples*. **(D,E)** Bar plots showing the amount of significantly up- and downregulated genes in ECT2/3 targets and non-targets. **(F,G)** List with the 10 most significantly enriched GO terms among significantly upregulated ECT2/3 targets (permissive set) (F), or downregulated non-targets (G) upon loss of ECT2/3/4 function.

Figure supplement 1. ECT2/3 targets are generally less abundant in root tips of *ect2/ect3/ect4* knockout plants.

analysis revealed that down-regulated ECT2/3 targets were particularly enriched in genes related to ribosome biogenesis and translation (*Figure 7F*), while upregulated non-targets were enriched in "abiotic stress responses" with molecular function "transcription factor" (*Figure 7G*). Because cell wall digestion required for protoplast isolation is a cellular stress, we tested the trivial possibility that loss of ECT2/3/4 function renders cells more susceptible to stress, and that such potential hyper-susceptibility underlies the observed differences of gene expression in ECT2-expressing root protoplasts. To this end, we isolated RNA from intact root apices of 4-day old plants of Col-0 wild type and *te234* mutants, and performed mRNA-seq analysis. These results recapitulated the trends of downregulation of stringent ECT2/3 targets and upregulation of stress-responsive non-targets, albeit with less pronounced differences than observed in the selected ECT2-expressing cell populations as expected (*Figure 7—figure supplement 1*). We also noticed that several stress-inducing and growth-restricting NF-YA-class transcription factors, all repressed by miR169defg, were upregulated in root tips (*Figure 8A*), and used small RNA-seq to test if activation of the stress response was visible in the miRNA expression profile. Indeed, the miR169defg family was specifically repressed in *te234* mutants, and the miR167 family, targeting growth-promoting auxin-response factors, was clearly upregulated (*Figure 8B*). In addition, the LTR-retrotransposon-targeting miR845a (Borges et al. 2018) was strongly upregulated. Thus, the stress response detected in *te234* mutants comprises coherent changes of miRNA and transcription factor expression. These data confirm that the observed patterns of differential gene expression in selected protoplasts are genuine and biologically meaningful, and that the selection of ECT2-expressing cells ensures the most accurate description of differential gene expression resulting from loss of ECT2/3/4 function. We note that while the differential gene expression analysis suggests that ECT2/3/4 formally act to increase abundance of their mRNA targets, it does not allow conclusions to be drawn on how such activation is brought about: a direct stabilizing effect of ECT2/3/4 binding to their targets is consistent with the observed results, but indirect effects via transcriptional repression cannot be excluded, especially given the presence of stress-related transcription factors in the set of up-regulated non-targets.

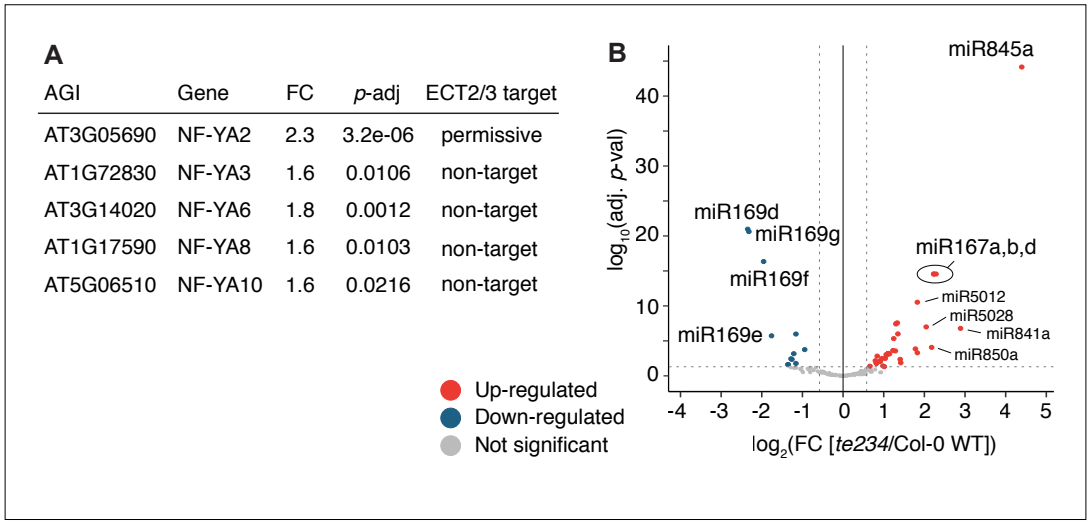

AGI	Gene	FC	*p*-adj	ECT2/3 target
AT3G05690	NF-YA2	2.3	3.2e-06	permissive
AT1G72830	NF-YA3	1.6	0.0106	non-target
AT3G14020	NF-YA6	1.8	0.0012	non-target
AT1G17590	NF-YA8	1.6	0.0103	non-target
AT5G06510	NF-YA10	1.6	0.0216	non-target

Figure 8. miRNA profile in root tips of *ect2/ect3/ect4* knockout plants. (A) Differential expression analysis of *te234* vs. Col-0 WT in 4-day-old root tips shows that expression of several stress-related NF-YA transcription factors (miR169defg targets) is induced in *te234* plants. FC, Fold Change [*te234*/WT]. **(B)** Volcano plot showing miRNAs differentially expressed in *te234* vs. Col-0 WT in 4-day-old root tips.

Discussion

Our identification and comparative analyses of mRNA targets of ECT2 (*accompanying manuscript*) and ECT3, and study of their behavior in terms of abundance and use of alternative polyadenylation in cell populations devoid of ECT2/3/4 activity allow us to draw two major conclusions. First, combining the overlapping expression patterns of ECT2 and ECT3, their formal genetic redundancy (Arribas-Hernández et al. 2018; Arribas-Hernández et al. 2020), their overlapping target sets, and the signatures of redundant target interaction derived from HyperTRIBE in single and triple *ect* mutant backgrounds, we conclude that many target mRNAs can bind to either ECT2 or ECT3 with similar consequences; i.e. ECT2 and ECT3 can exhibit redundant function *sensu stricto*, not just the ability to replace function in the absence of the other protein. Second, ECT2 is not nuclear, and ECT2/3/4 do not appreciably affect alternative polyadenylation in their direct mRNA targets. It is important to note that this conclusion on ECT2/3/4 does not extend to m^6A altogether. Polyadenylation and transcription termination are clearly influenced by m^6A in plants, as shown by studies of mutants in core *N6*-adenosine methyltransferase components VIR and FIP37. In *vir-1* mutants, a tendency to use proximal alternative PASs in m^6A-targets is prominent (Parker et al. 2020), and in *fip37* mutants, several cases of defective transcription termination causing production of chimeric transcripts were noted (Pontier et al. 2019). In the latter case, m^6A recognition by the YTHDC-containing nuclear subunit of the Cleavage and Polyadenylation Specificity Factor CPSF30 was demonstrated to be required for regular transcription termination, and subsequent studies of CPSF30, including of mutants specifically defective in m^6A-binding, also indicated its role in mediating m^6A-dependent alternative polyadenylation (Hou et al. 2021; Song et al. 2021). Thus, m^6A does affect 3'-end formation of methylated pre-mRNAs in plants, but this process involves the nuclear CPSF30 which contains a YTHDC domain only in plants, rather than the cytoplasmic YTHDF protein ECT2.

The immediate implication of the conclusions that ECT2 does not act in the nucleus and does not influence alternative polyadenylation is that the conceptual framework for m^6A-YTHDF action established mostly through studies in mammalian cell culture does extend to plants: m^6A is installed by a nuclear methyltransferase complex (Zhong et al. 2008; Shen et al. 2016; Růžička et al. 2017), probably coupled to RNA Polymerase II transcription (Bhat et al. 2020), and YTHDF-mediated regulation of transcripts carrying the m^6A mark takes place in the cytoplasm. Then, what is the molecular effect of ECT2/ECT3-binding to target mRNAs? Clearly, lack of ECT2/3/4 results in decreased abundance of direct targets. This result is in line with the lower accumulation of m^6A-containing transcripts observed in plants partially depleted of m^6A (Shen et al. 2016; Anderson et

al. 2018; Parker et al. 2020) and in the *ect2-1* knockout line (Wei et al. 2018) compared to wild type plants. However, differential expression analysis of ubiquitously expressed targets performed with RNA from entire plants is not easy to interpret when the regulatory process subject to study is located only in well-defined cell populations of meristematic tissues (Zhong et al. 2008; Arribas-Hernández et al. 2018; Arribas-Hernández et al. 2020). The problem is even more acute when the tissue composition of wild type and mutant individuals to be compared is different due to the developmental delay of the m^6A-deficient lines. Lastly, some of the previous studies of differential gene expression also revealed a number of m^6A-containing transcripts with increased abundance in m^6A-deficient mutants (Shen et al. 2016; Anderson et al. 2018), of which some were proposed to be of importance for the observed phenotype (Shen et al. 2016). Thus, the studies on differential gene expression in m^6A-deficient mutants compared to wild type published thus far do not allow clear conclusions on the consequence of loss of m^6A (or a reader protein) for target mRNA accumulation to be drawn (Arribas-Hernández and Brodersen 2020). In contrast, our experimental setup, using a tissue with comparable cell-type composition in wild type and mutant plants and extracting RNA only from the cells in which target regulation by ECT2/3/4 takes place, establishes that targets generally have decreased abundance upon loss of ECT2/3/4.

The present study does not, however, elucidate the mechanisms involved in target regulation, because it does not directly measure target mRNA synthesis and degradation rates. It is possible that the reduced target mRNA accumulation in *ect2/3/4* mutant cells is exclusively a direct consequence of ECT2/3/4 function at the post-transcriptional level, for example mRNA stabilization by protection from endonucleolysis as previously suggested (Anderson et al. 2018). We cannot at present exclude, however, that more indirect effects also play a role, perhaps related to transcriptional repression of ECT2/3/4 targets via stress responses activated upon loss of ECT2/3/4 function. We anticipate that clear answers to this question must await development of tools for conditional inactivation of ECT2/3 function, such that consequences for mRNA target fate can be studied immediately after loss of ECT2/3 binding. We also note that the constitutive stress response activation is consistent with the stunted phenotype of *te234* mutants (Arribas-Hernández et al. 2018; Arribas-Hernández et al. 2020). Thus, disentangling direct effects of ECT2/3/4 on growth via mRNA target regulation from possible indirect effects arising from stress response activation in knockout mutants will be of major importance in future studies.

Methods

All data analyses were carried out using TAIR 10 as the reference genome and Araport11 as the reference transcriptome. Unless otherwise stated, data analyses were performed in R (https://www.R-project.org/) and plots generated using either base R or ggplot2. (https://ggplot2.tidyverse.org).

Plant material

All lines employed in this study are in the *Arabidopsis thaliana* Col-0 ecotype. The mutant alleles or their combinations: *ect2-1* (SALK_002225) (Arribas-Hernández et al. 2018; Scutenaire et al. 2018; Wei et al. 2018), *ect3-1* (SALKseq_63401), *ect4-2* (GK_241H02), and *ect2-1/ect3-1/ect4-2* (*te234*) (Arribas-Hernández et al. 2018) have been previously described. The transgenic lines *ect2-1 ECT2-FLAG-ADAR* and *te234 ECT2-FLAG-ADAR* (*accompanying manuscript*), *GFP:WIP1* (Xu et al. 2007) and those expressing *ECT2pro:ECT2-mCherry-ECT2ter* and *ECT2pro:ECT2^{W464A}-mCherry-ECT2ter* (Arribas-Hernández et al. 2018; Arribas-Hernández et al. 2020) have also been described. Plants co-expressing *ECT2-mCherry* and GFP-*WIP1* used for fluorescence microscopy were the F1 progeny of a genetic cross between GFP-*WIP1* and *ECT2-mCherry*-expressing plants.

Growth conditions

Seeds were surface-sterilized by 2-min incubation in 70% EtOH plus 10 min in [1.5% NaOCl, 0.05% Tween-20], two H_2O washes, and 2-5 days of stratification at 4°C in darkness. To harvest tissue for HyperTRIBE experiments, and for the PASs and differential expression analyses, we grew seedlings in vertically disposed plates with Murashige and Skoog (MS)-agar medium (4.4 g/L MS, 10 g/L sucrose, 10 g/L agar; pH 5.7) at 20°C, receiving ~70 µmol m^{-2} s^{-1} of light in a 16 hr light/8 hr dark cycle. Conditions were identical to those used for ECT2-HyperTRIBE and iCLIP experiments (*accompanying manuscript*). To assess phenotypes of the lines employed for ECT3-HT, we grew seedlings in horizontal MS plates (4.4 g/L MS, 10 g/L sucrose, 8 g/L agar; pH 5.7) at 21ºC in the same light regime, transferred to soil ~8 days after germination, and maintained in Percival incubators also under long day conditions.

Definitions of experiment, biological replicates and technical replicates

We use the term “biological replicate” in the following way: Plants were grown at the same time, under the same conditions, but in separate plates. Each sample replicate contains pools of seedlings prepared in such a way that no two replicates contains seedlings grown on the same

plates. This sampling ensures that plate-to-plate variation in growth conditions, if any, will have an effect on measurements of gene expression within a single genotype, and hence minimize the risk that any differences due to such variation are called as significant in comparisons between genotypes.

"Technical replicates" are understood to be independently conducted measurements using the same technique on the same biological material (e.g. on one biological replicate as defined above). Technical replicates were not carried out in this study, and the term "replicate" refers to biological replicate as defined above.

In our definition, an "experiment" results in generation and comparison of measurements arising from multiple biological replicates of different biological entities, in the present case often *Arabidopsis* seedlings differing in genotype with respect to the genes *ECT2*, *ECT3* and *ECT4*. Thus, repetition of an experiment in our definition entails generation and analysis of the required biological replicates at different points in time.

Generation of transgenic lines for ECT3-HyperTRIBE

We generated lines expressing *ECT3pro:ECT3-FLAG-ADAR-ECT3ter* and *ECT3pro:FLAG-ADAR-ECT3ter* by USER cloning (Bitinaite and Nichols 2009) and agrobacterium-mediated transformation in the same way as for the ECT2 equivalents (*accompanying manuscript*). Primer sequences are detailed in *Table 1*. We selected 5 independent lines of each type based on segregation studies (to isolate single T-DNA insertions), phenotypic complementation (in the *te234* background) and transgene expression levels assessed by FLAG western blot.

HyperTRIBE

The HyperTRIBE experiments were performed once, using 5 biological replicates (independent lines) for each of the groups (genotypes) used. Growth conditions and experimental procedures were identical for all the groups compared in this study. Root and aerial tissue were dissected from the same plants in all cases. Tissue dissection, RNA extraction and library preparation were done as described for ECT2-HyperTRIBE in the *accompanying manuscript*. Briefly, we Trizol-extracted total RNA from manually dissected root tips and apices (removing cotyledons) of 10-day-old T2 seedlings. After mRNA enrichment with oligo(dT) beads (18-mers), Illumina mRNA-Seq libraries were then prepared by Novogene.

Analysis of HyperTRIBE data

Significant differentially edited sites between *ECT3-FLAG-ADAR* (fusion) and *FLAG-ADAR* (control) samples were called according to our hyperTRIBE**R** pipeline (https://github.com/sarah-ku/hyperTRIBER) as described for ECT2-HyperTRIBE in the *accompanying manuscript*, without removal of any sample.

For the analysis of editing sites by ECT2/3-FLAG-ADAR in triple (*te234*) vs. single (either *ect2-1* or *ect3-1*) mutant background, the hyperTRIBE**R** pipeline was run between the two types of samples without taking into account the free ADAR controls, in order to detect positions edited preferentially in one or the other background. To account for low power as a result of high variance in editing proportions due to transgene expression differences across samples, scaled ADAR abundance was treated as an extra co-variate in the model. This resulted in enriched sensitivity to specifically call A-to-G positions, which were subsequently considered as significant if they had an adjusted *p*-value < 0.1 and an absolute $\log_2$(fold change) > 0.25. We also required positions to be a significantly edited site in at least one of the single or triple mutant set ups against the free FLAG-ADAR control samples.

Comparison with root single cell data

The expression matrix based on a total of 4727 individual cells from scRNA-seq in roots was downloaded from Denyer et al. (2019), together with extensive lists of marker genes associated with 15 clusters annotated to cell types in roots. To calculate the proportion of markers at target genes: for each of the 15 clusters, the proportion of marker genes that are ECT2 or ECT3 targets (based on ECT2-HT and ECT3-HT respectively in roots) was calculated. Proportions were then overlayed onto a t-SNE diagram (Denyer et al. 2019), according to relevant clusters of cells.

Preparation and sorting of protoplasts

We harvested roots from 5-day-old T4 seedlings grown on vertical square plates (20 plates with 4 rows of densely spotted seeds in each plate per line/replicate) to digest in 20 mL of protoplasting solution (20 mM MES, 0.4 M D-Mannitol, 20 mM KCl, 1.25% w/v Cellulase, 0.3% Macerozyme, 0.1% w/v BSA, 10 mM CaCl2, 5mM β-mercaptoethanol; pH 5.7), following Benfey's lab procedure (Birnbaum et al. 2005; Bargmann and Birnbaum 2010). After the 75 min of incubation at 27ºC with gentle agitation, we filtered the cell-suspensions through a 40 µm strainer and pelleted cells by centrifugation at 500 *g* for 10 min at room temperature in a swinging-bucket centrifuge. Pellets were gently resuspended in 400 µL of protoplasting solution for direct sorting in a FACSAriaIII cytometer.

The flow stream was adjusted to 20 psi sheath pressure with a 100 µm nozzle aperture. Sorted cells were collected into RTL buffer supplemented with 40 mM DTT (3.5 vol of buffer per volume of cell suspension) and lysed by vortexing. The protoplast extracts were flash-frozen on dry ice until extraction with the RNeasy Plus Micro kit (QIAGEN) following the manufacturer's instructions. The yield was ~300.000 cells in a volume of 1.5 mL (per sample). Samples were harvested, prepared and sorted with a 15 min. lapse between them to account for sorting time. In that way, every sample was processed in the same amount of time (~2 h from the start of harvesting to sorting). To prevent any possible bias, the samples of each genotype (3+3) were alternated during all the processing.

Smart-seq2

Smart-seq2 libraries were generated according to Picelli *et al.* (2013) using the Illumina DNA Nextera Flex kit from total RNA extracted with the RNeasy Plus Micro kit (QIAGEN) from FACS-sorted root protoplasts (Birnbaum et al. 2005). The libraries were sequenced in PE75 mode on an Illumina NextSeq550 sequencer. Nextera transposase adapters were trimmed from all reads using Cutadapt.

Polyadenylation Site Analysis

Smart-seq2 reads with at least 9 3'-terminal A nucleotides or 5'-terminal T nucleotides were labelled as putative poly(A)-containing reads and the oligo-A/T sequences were removed with a maximum allowed mismatch rate of 6%. All putative poly(A)-containing reads with a length >20 and a mean quality score >25 after trimming were retained along with their mate pair and mapped to the *Arabidopsis thaliana* TAIR10 genome using STAR with the following parameters:

--alignIntronMax 5000 --alignMatesGapMax 5500 --outFilterMatchNmin 20
--alignSJDBoverhangMin 1 --outFilterMismatchNmax 5
--outFilterMismatchNoverLmax .05 --outFilterType BySJout
--outFilterIntronMotifs RemoveNoncanonicalUnannotated

Putative poly(A)-containing reads that mapped to the genome were filtered for false positives by examining the adjacent nucleotides in the genome: reads were removed if the putative poly(A) site was immediately upstream of a 15nt region that is at least 80% purines (which are likely sites of oligo-dT mispriming). All putative poly(A)-containing reads not filtered in this way were retained as poly(A) sites and were counted for each position in the genome based on the most 3' nucleotide of each read (allowing 3'-terminal mismatches).

Polyadenylation site clusters (PACs) were identified using a modification of the nanoPARE analysis

pipeline (https://github.com/Gregor-Mendel-Institute/nanoPARE) (Schon et al. 2018). Briefly, reads from the samples above that did not contain untemplated poly(A) tails were mapped to the genome and used as a negative control of "gene body reads". Then, subtractive kernel density estimation was performed for each sample using *endGraph.sh* with default settings to produce a BED file for each sample containing poly(A) site clusters. As a final filter against oligo-dT mispriming events, the reads removed as false positives in the previous step that overlap with each cluster were counted. If the cluster contained more filtered signal than unfiltered signal, the entire cluster was considered a false positive cluster. Clusters were retained if an overlapping site was identified in at least 2 of the 3 replicates of both *ect2-1 ECT2-mCherry* and *te234 ECT2*^{W464A}*-mCherry* genotypes. These two sets of clusters were merged using *bedtools merge*. Clusters mapping to the mitochondrial and chloroplast genome and the 2 rDNA loci were discarded, and the rest were retained for quantification.

mRNA-Seq and small RNA-Seq from root tips

Total RNA purified from manually dissected root tips of 4-day-old plants (using the same growing conditions and methodology as for the HyperTRIBE lines) was used for preparation of Illumina mRNA-Seq (same methodology as for HyperTRIBE) and small RNA-Seq libraries (NEBNext small RNA library prep set). The experiment was performed once, using 3 biological replicates for mRNA-Seq, and 2 for small RNA-Seq.

Differential expression analysis (mRNA and miRNAs)

Differential gene expression analysis of mRNA was performed from processed and quantified Smart-seq2 or RNA-Seq data using DESeq2 (Love et al. 2014), for all genes with at least 1 TPM in all six samples (three biological replicates of the two types) and a total sum of at least 5 TPM. Significantly differentially expressed genes (FDR < 0.05) were considered to be upregulated in the mutants if the fold change between mutant and wild type samples was higher than 1.5, or downregulated if lower than 1/1.5.

For small RNA-Seq, raw reads were trimmed with cutadapt v3.4 (Kechin et al. 2017) to lengths of 18-28 nt, and mapped to the *Arabidopsis* genome using STAR v2.6.0a (Dobin et al. 2013) with genome indexes built on the Araport11_GTF_genes_transposons.Mar202021.gtf annotation. Mapped reads were counted using featureCounts v2.0.1 (Liao et al. 2014). Genes with less than 1 RPM in all four samples (two biological replicates of the two types) were excluded from the analysis. Differential expression analysis was conducted using DESeq2 version 1.28.1 (Love et

592 al. 2014) on the resulting matrix. Genes with adjusted p-value (FDR) lower or equal to 0.05 were
593 considered significantly differentially expressed, and upregulated in *te234* mutants if the fold
594 change between *te234* and *Col-0 WT* samples was higher than 1.5, or downregulated if lower than
595 1/1.5.
596
597 *GO Term enrichment analysis*
598 The functional enrichment analysis was carried out using the R package gprofiler2 version 0.2.0
599 (Raudvere et al. 2019).
600
601 *Fluorescence Microscopy*
602 Entire root tips growing inside MS-agar plates were imaged with a Leica MZ16 F stereomicroscope
603 with a Sony α6000 camera. Standard confocal fluorescence microscopy images of cells in root
604 meristems were acquired with a Zeiss LSM700 confocal microscope as described in Arribas-
605 Hernández et al. (2018) using ~7-day-old seedlings grown on MS-agar plates and freshly mounted
606 in water. For super-resolution fluorescence microscopy, we used a Zeiss LSM900 equipped with
607 the Airyscan detector (Huff 2015). Fluorescence intensity plots were obtained with the tool “Plot
608 Profile” of the image-processing package ImageJ (Schindelin et al. 2012).
609

Data Access

Accession numbers

The raw and processed data for ECT3-HyperTRIBE, Smart-seq2 from root protoplasts and RNA-seq from root tips have been deposited in the European Nucleotide Archive (ENA) at EMBL-EBI under the accession number PRJEB44359.

Code availability

The code for running the hyperTRIBE**R** pipeline is available at https://github.com/sarah-ku/targets_arabidopsis, and the nanoPARE pipeline for PAS analysis can be found at https://github.com/Gregor-Mendel-Institute/nanoPARE.

Acknowledgements

We thank Lena Bjørn Johansson and Phillip Andersen for technical assistance in the construction of transgenic lines, Emilie Oksbjerg for preparing and sequencing small RNA libraries, Theo Bølsterli, René Hvidberg Petersen and their teams for plant care, and Anna Fossum and Rajesh Somasundaram for their assistance with FACS. Kim Rewitz and Kenneth Halberg are thanked for assistance with Airyscan microscopy. We acknowledge Mathias Tankmar, Alexander J.H. Andersen and Freja Asmussen for experimental support, and Tom Denyer and Marja Timmermans for their input and support in the analyses of ECT2/3 expression and target enrichment in their scRNAseq data. We are grateful to Norman R. Groves and Iris Meier for the kind donation of GFP-WIP1 seeds. This work was supported by a Consolidator Grant from the European Research Council (PATHORISC, ERC-2016-COG 726417) and a Research Grant from the Independent Research Fund Denmark (9040-00409B) to P.B.; a Starting Grant from the European Research Council (638173) and a Sapere Aude Starting Grant from the Independent Research Fund Denmark (6108-00038B) to R.A.; and a European Research Council under the European Union's Horizon 2020 Research and Innovation Program grant 63788 to M.N.

Author Contributions

P.B. and L.A.-H. designed and coordinated the study. L.A.-H. built the biological material for ECT3-HT. S.R. called edited sites to define ECT3-HT target sets and compared the ECT2 and ECT3-HT datasets. L.A.-H. produced protoplast and root tip RNA samples, B.E. generated Smart-seq2 libraries, M.S. analyzed poly(A) sites, and C.P. performed differential expression of mRNA and miRNA, and GO-term enrichment analyses. M.N. supervised work related to PAS mapping. P.B. and L.A.-H. wrote the manuscript with input from all authors.

644 **References**

645

646 Anderson SJ, Kramer MC, Gosai SJ, Yu X, Vandivier LE, Nelson ADL, Anderson ZD, Beilstein MA,
647 Fray RG, Lyons E et al. 2018. N(6)-Methyladenosine Inhibits Local Ribonucleolytic Cleavage to
648 Stabilize mRNAs in Arabidopsis. *Cell Rep* **25**: 1146-1157.

649 Arribas-Hernández L, Bressendorff S, Hansen MH, Poulsen C, Erdmann S, Brodersen P. 2018. An
650 m6A-YTH Module Controls Developmental Timing and Morphogenesis in Arabidopsis. *Plant Cell*
651 **30**: 952-967.

652 Arribas-Hernández L, Brodersen P. 2020. Occurrence and functions of m6A and other covalent
653 modifications in plant mRNA. *Plant Physiol* **182**: 79-96.

654 Arribas-Hernández L, Simonini S, Hansen MH, Paredes EB, Bressendorff S, Dong Y, Østergaard L,
655 Brodersen P. 2020. Recurrent requirement for the m6A-ECT2/ECT3/ECT4 axis in the control of
656 cell proliferation during plant organogenesis. *Development* **147**: dev189134.

657 Balacco DL, Soller M. 2019. The m6A Writer: Rise of a Machine for Growing Tasks. *Biochemistry*
658 **58**: 363-378.

659 Bargmann BOR, Birnbaum KD. 2010. Fluorescence Activated Cell Sorting of Plant Protoplasts.
660 *JoVE* doi:doi:10.3791/1673: e1673.

661 Bhat SS, Bielewicz D, Gulanicz T, Bodi Z, Yu X, Anderson SJ, Szewc L, Bajczyk M, Dolata J,
662 Grzelak N et al. 2020. mRNA adenosine methylase (MTA) deposits m⁶A on
663 pri-miRNAs to modulate miRNA biogenesis in Arabidopsis thaliana. *Proc Natl*
664 *Acad Sci USA* **117**: 21785.

665 Birnbaum K, Jung JW, Wang JY, Lambert GM, Hirst JA, Galbraith DW, Benfey PN. 2005. Cell
666 type–specific expression profiling in plants via cell sorting of protoplasts from fluorescent reporter
667 lines. *Nat Meth* **2**: 615-619.

668 Bitinaite J, Nichols NM. 2009. DNA cloning and engineering by uracil excision. *Curr Protoc Mol Biol*
669 **Chapter 3**: Unit 3 21.

670 Borges F, Parent J-S, van Ex F, Wolff P, Martínez G, Köhler C, Martienssen RA. 2018.
671 Transposon-derived small RNAs triggered by miR845 mediate genome dosage response in
672 Arabidopsis. *Nat Genet* **50**: 186-192.

673 Denyer T, Ma X, Klesen S, Scacchi E, Nieselt K, Timmermans MCP. 2019. Spatiotemporal
674 Developmental Trajectories in the Arabidopsis Root Revealed Using High-Throughput Single-Cell
675 RNA Sequencing. *Dev Cell* **48**: 840-852.e845.

676 Dobin A, Davis CA, Schlesinger F, Drenkow J, Zaleski C, Jha S, Batut P, Chaisson M, Gingeras
677 TR. 2013. STAR: ultrafast universal RNA-seq aligner. *Bioinformatics* **29**: 15-21.

678 Dominissini D, Moshitch-Moshkovitz S, Schwartz S, Salmon-Divon M, Ungar L, Osenberg S,
679 Cesarkas K, Jacob-Hirsch J, Amariglio N, Kupiec M et al. 2012. Topology of the human and
680 mouse m6A RNA methylomes revealed by m6A-seq. *Nature* **485**: 201-206.

681 Hou Y, Sun J, Wu B, Gao Y, Nie H, Nie Z, Quan S, Wang Y, Cao X, Li S. 2021. CPSF30-L-
682 mediated recognition of mRNA m6A modification controls alternative polyadenylation of nitrate
683 signaling-related gene transcripts in Arabidopsis. *Molecular Plant* doi:10.1016/j.molp.2021.01.013.

684 Huff J. 2015. The Airyscan detector from ZEISS: confocal imaging with improved signal-to-noise
685 ratio and super-resolution. *Nat Meth* **12**: i-ii.

686 Kechin A, Boyarskikh U, Kel A, Filipenko M. 2017. cutPrimers: A New Tool for Accurate Cutting of
687 Primers from Reads of Targeted Next Generation Sequencing. *J Comput Biol* **24**: 1138-1143.

688 König J, Zarnack K, Rot G, Curk T, Kayikci M, Zupan B, Turner DJ, Luscombe NM, Ule J. 2010.
689 iCLIP reveals the function of hnRNP particles in splicing at individual nucleotide resolution. *Nat*
690 *Struct Mol Biol* **17**: 909-915.

691 Kontur C, Jeong M, Cifuentes D, Giraldez AJ. 2020. Ythdf m6A Readers Function Redundantly
692 during Zebrafish Development. *Cell Rep* **33**: 108598.

693 Lasman L, Krupalnik V, Viukov S, Mor N, Aguilera-Castrejon A, Schneir D, Bayerl J, Mizrahi O,
694 Peles S, Tawil S et al. 2020. Context-dependent functional compensation between Ythdf m6A
695 reader proteins. *Genes Dev* **34**: 1373-1391.

696 Li A, Chen Y-S, Ping X-L, Yang X, Xiao W, Yang Y, Sun H-Y, Zhu Q, Baidya P, Wang X et al. 2017.
697 Cytoplasmic m6A reader YTHDF3 promotes mRNA translation. *Cell Res* **27**: 444.

698 Li D, Zhang H, Hong Y, Huang L, Li X, Zhang Y, Ouyang Z, Song F. 2014a. Genome-wide
699 identification, biochemical characterization, and expression analyses of the YTH domain-
700 containing RNA-binding protein family in Arabidopsis and rice. *Plant Mol Biol Report* **32**: 1169-
701 1186.

702 Li F, Zhao D, Wu J, Shi Y. 2014b. Structure of the YTH domain of human YTHDF2 in complex with
703 an m6A mononucleotide reveals an aromatic cage for m6A recognition. *Cell Res* **24**: 1490-1492.

704 Li M-W, Zhou L, Lam H-M. 2015. Paraformaldehyde Fixation May Lead to Misinterpretation of the
705 Subcellular Localization of Plant High Mobility Group Box Proteins. *PLOS ONE* **10**: e0135033.

706 Liao Y, Smyth GK, Shi W. 2014. featureCounts: an efficient general purpose program for assigning
707 sequence reads to genomic features. *Bioinformatics* **30**: 923-930.

708 Love MI, Huber W, Anders S. 2014. Moderated estimation of fold change and dispersion for RNA-
709 seq data with DESeq2. *Genome biology* **15**: 550.

710 Luo S, Tong L. 2014. Molecular basis for the recognition of methylated adenines in RNA by the
711 eukaryotic YTH domain. *Proc Natl Acad Sci USA* **111**: 13834-13839.

712 Ma X, Denyer T, Timmermans MCP. 2020. PscB: A Browser to Explore Plant Single Cell RNA-
713 Sequencing Data Sets1[OPEN]. *Plant Physiol* **183**: 464-467.

714 McMahon Aoife C, Rahman R, Jin H, Shen James L, Fieldsend A, Luo W, Rosbash M. 2016.
715 TRIBE: Hijacking an RNA-Editing Enzyme to Identify Cell-Specific Targets of RNA-Binding
716 Proteins. *Cell* **165**: 742-753.

Parker MT, Knop K, Sherwood AV, Schurch NJ, Mackinnon K, Gould PD, Hall AJW, Barton GJ, Simpson GG. 2020. Nanopore direct RNA sequencing maps the complexity of Arabidopsis mRNA processing and m6A modification. *eLife* **9**: e49658.

Patil DP, Pickering BF, Jaffrey SR. 2018. Reading m6A in the Transcriptome: m6A-Binding Proteins. *Trends Cell Biol* **28**: 113-127.

Picelli S, Björklund ÅK, Faridani OR, Sagasser S, Winberg G, Sandberg R. 2013. Smart-seq2 for sensitive full-length transcriptome profiling in single cells. *Nat Meth* **10**: 1096-1098.

Pontier D, Picart C, El Baidouri M, Roudier F, Xu T, Lahmy S, Llauro C, Azevedo J, Laudié M, Attina A et al. 2019. The m6A pathway protects the transcriptome integrity by restricting RNA chimera formation in plants. *Life Science Alliance* **2**: e201900393.

Raudvere U, Kolberg L, Kuzmin I, Arak T, Adler P, Peterson H, Vilo J. 2019. g:Profiler: a web server for functional enrichment analysis and conversions of gene lists (2019 update). *Nucleic Acids Res* **47**: W191-W198.

Růžička K, Zhang M, Campilho A, Bodi Z, Kashif M, Saleh M, Eeckhout D, El-Showk S, Li H, Zhong S et al. 2017. Identification of factors required for m6A mRNA methylation in Arabidopsis reveals a role for the conserved E3 ubiquitin ligase HAKAI. *New Phytol* **215**: 157-172.

Schindelin J, Arganda-Carreras I, Frise E, Kaynig V, Longair M, Pietzsch T, Preibisch S, Rueden C, Saalfeld S, Schmid B et al. 2012. Fiji: an open-source platform for biological-image analysis. *Nat Meth* **9**: 676-682.

Schon MA, Kellner MJ, Plotnikova A, Hofmann F, Nodine MD. 2018. NanoPARE: parallel analysis of RNA 5' ends from low-input RNA. *Genome Res* **28**: 1931-1942.

Scutenaire J, Deragon J-M, Jean V, Benhamed M, Raynaud C, Favory J-J, Merret R, Bousquet-Antonelli C. 2018. The YTH Domain Protein ECT2 Is an m6A Reader Required for Normal Trichome Branching in Arabidopsis. *Plant Cell* **30**: 986-1005.

Shen L, Liang Z, Gu X, Chen Y, Teo Zhi Wei N, Hou X, Cai Weiling M, Dedon Peter C, Liu L, Yu H. 2016. N6-methyladenosine RNA modification regulates shoot stem cell fate in Arabidopsis. *Dev Cell* **38**: 186-200.

Sherstnev A, Duc C, Cole C, Zacharaki V, Hornyik C, Ozsolak F, Milos PM, Barton GJ, Simpson GG. 2012. Direct sequencing of Arabidopsis thaliana RNA reveals patterns of cleavage and polyadenylation. *Nat Struct Mol Biol* **19**: 845-852.

Shi H, Wang X, Lu Z, Zhao BS, Ma H, Hsu PJ, Liu C, He C. 2017. YTHDF3 facilitates translation and decay of N6-methyladenosine-modified RNA. *Cell Res* **27**: 315-328.

Song P, Yang J, Wang C, Lu Q, Shi L, Tayier S, Jia G. 2021. Arabidopsis N6methyladenosine reader CPSF30-L recognizes FUE signals to control polyadenylation site choice in liquid-like nuclear bodies. *Molecular Plant* doi:10.1016/j.molp.2021.01.014.

Stoilov P, Rafalska I, Stamm S. 2002. YTH: a new domain in nuclear proteins. *Trends Biochem Sci* **27**: 495-497.

754 Tanious FA, Veal JM, Buczak H, Ratmeyer LS, Wilson WD. 1992. DAPI (4',6-diamidino-2-
755 phenylindole) binds differently to DNA and RNA: minor-groove binding at AT sites and
756 intercalation at AU sites. *Biochemistry* **31**: 3103-3112.

757 Theler D, Dominguez C, Blatter M, Boudet J, Allain FH. 2014. Solution structure of the YTH domain
758 in complex with N6-methyladenosine RNA: a reader of methylated RNA. *Nucleic Acids Res* **42**:
759 13911-13919.

760 Wang X, Lu Z, Gomez A, Hon GC, Yue Y, Han D, Fu Y, Parisien M, Dai Q, Jia G et al. 2014. N6-
761 methyladenosine-dependent regulation of messenger RNA stability. *Nature* **505**: 117-120.

762 Wang X, Zhao Boxuan S, Roundtree Ian A, Lu Z, Han D, Ma H, Weng X, Chen K, Shi H, He C.
763 2015. N6-methyladenosine modulates messenger RNA translation efficiency. *Cell* **161**: 1388-
764 1399.

765 Wei L-H, Song P, Wang Y, Lu Z, Tang Q, Yu Q, Xiao Y, Zhang X, Duan H-C, Jia G. 2018. The m6A
766 Reader ECT2 Controls Trichome Morphology by Affecting mRNA Stability in Arabidopsis. *Plant*
767 *Cell* **30**: 968-985.

768 Worpenberg L, Paolantoni C, Longhi S, Mulorz MM, Lence T, Wessels H-H, Dassi E, Aiello G,
769 Sutandy FXR, Scheibe M et al. 2021. Ythdf is a N6-methyladenosine reader that modulates Fmr1
770 target mRNA selection and restricts axonal growth in Drosophila. *EMBO J* **40**: e104975.

771 Wu X, Liu M, Downie B, Liang C, Ji G, Li QQ, Hunt AG. 2011. Genome-wide landscape of
772 polyadenylation in Arabidopsis provides evidence for extensive alternative polyadenylation. *Proc*
773 *Natl Acad Sci USA* **108**: 12533.

774 Xu C, Wang X, Liu K, Roundtree IA, Tempel W, Li Y, Lu Z, He C, Min J. 2014. Structural basis for
775 selective binding of m6A RNA by the YTHDC1 YTH domain. *Nat Chem Biol* **10**: 927-929.

776 Xu W, Rahman R, Rosbash M. 2018. Mechanistic implications of enhanced editing by a
777 HyperTRIBE RNA-binding protein. *RNA* **24**: 173-182.

778 Xu XM, Rose A, Muthuswamy S, Jeong SY, Venkatakrishnan S, Zhao Q, Meier I. 2007. NUCLEAR
779 PORE ANCHOR, the Arabidopsis homolog of Tpr/Mlp1/Mlp2/megator, is involved in mRNA export
780 and SUMO homeostasis and affects diverse aspects of plant development. *Plant Cell* **19**: 1537-
781 1548.

782 Zaccara S, Jaffrey SR. 2020. A Unified Model for the Function of YTHDF Proteins in Regulating
783 m(6)A-Modified mRNA. *Cell* **181**: 1582-1595.e1518.

784 Zaccara S, Ries RJ, Jaffrey SR. 2019. Reading, writing and erasing mRNA methylation. *Nat Rev*
785 *Mol Cell Biol* **20**: 608-624.

786 Zhao BS, Roundtree IA, He C. 2017. Post-transcriptional gene regulation by mRNA modifications.
787 *Nat Rev Mol Cell Biol* **18**: 31.

788 Zhong S, Li H, Bodi Z, Button J, Vespa L, Herzog M, Fray RG. 2008. MTA is an Arabidopsis
789 messenger RNA adenosine methylase and interacts with a homolog of a sex-specific splicing
790 factor. *Plant Cell* **20**: 1278-1288.

Zhu T, Roundtree IA, Wang P, Wang X, Wang L, Sun C, Tian Y, Li J, He C, Xu Y. 2014. Crystal structure of the YTH domain of YTHDF2 reveals mechanism for recognition of N6-methyladenosine. *Cell Res* **24**: 1493-1496.

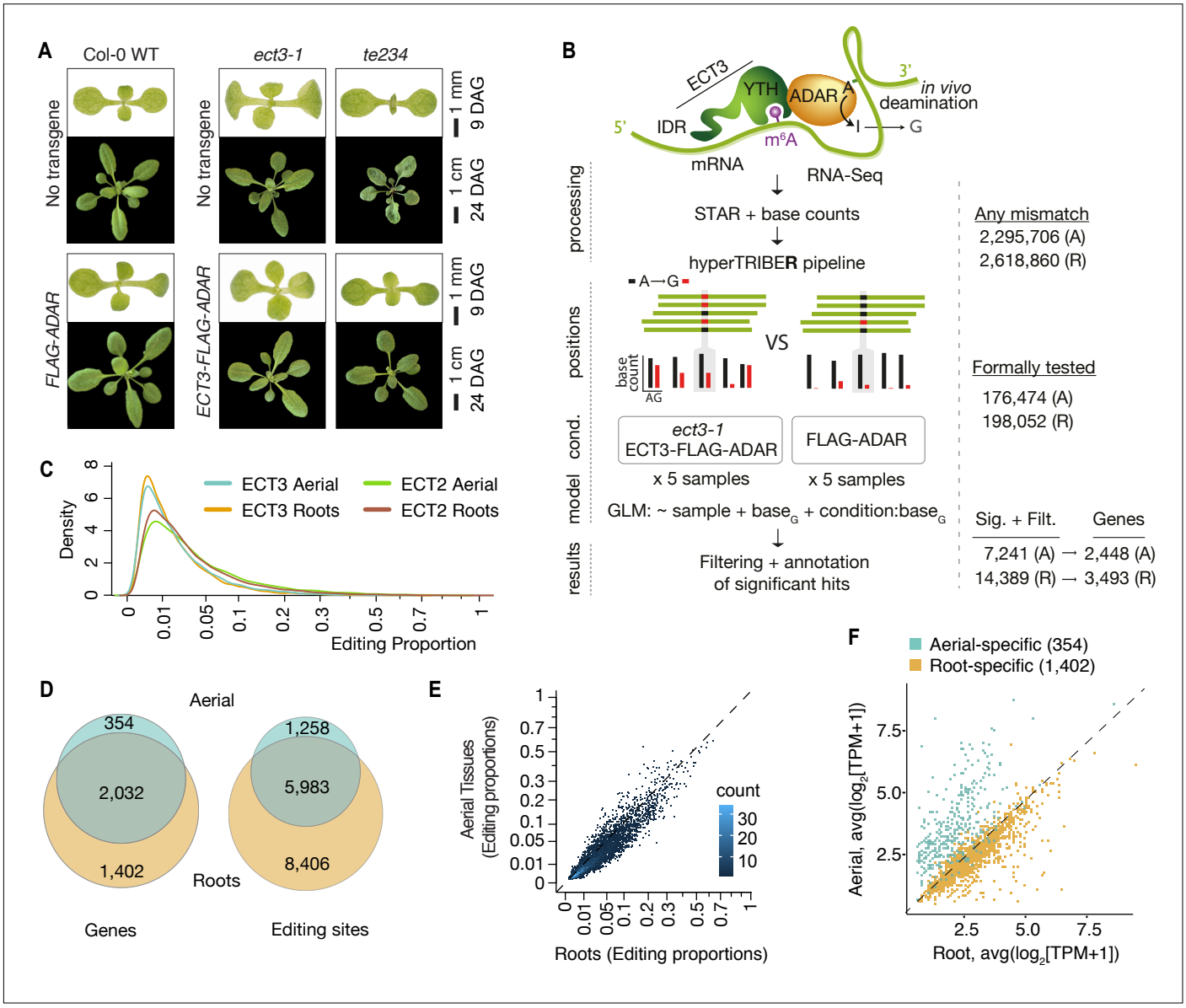

Figure 1. Identification of ECT3 targets using HyperTRIBE. (A) Phenotypes of wild type, *ect3-1* and *te234* (*ect2-1/ect3-1/ect4-2*) mutants with (lower panels) or without (upper panels) *ECT3pro:ECT3-FLAG-DmADAR^{E488Q}cd-ECT3ter* (*ECT3-FLAG-ADAR*) or *ECT3pro:FLAG-DmADAR^{E488Q}cd-ECT3ter* (*FLAG-ADAR*) transgenes, at 9 or 24 days after germination (DAG). **(B)** Experimental design for ECT3-HyperTRIBE (ECT3-HT) target identification. After quantifying nucleotide base counts from mapped RNA-seq libraries of *ect3-1 ECT3-FLAG-ADAR* and *FLAG-ADAR* lines, all positions with mismatches were passed into the HyperTRIBE**R** pipeline to call significant editing sites. Identified sites were further filtered to remove SNPs and retain only A-to-G mismatches. The number of sites in either aerial (A, dissected apices) or root (R, root tips) tissues at each stage is indicated. GLM, generalized linear model. **(C)** Density of editing proportions for significant editing sites in aerial tissues and roots of *ect3-1/ECT3-FLAG-ADAR* and *ect2-1/ECT2-FLAG-ADAR* (*accompanying manuscript*) lines. **(D)** Overlap between ECT3-HT target genes and editing sites in roots and aerial tissues, out of the set of genes commonly expressed in both tissues. **(E)** Scatterplot of the editing proportions of significant editing sites in ECT3-HT for aerial vs root tissues. **(G)** Scatterplot showing the expression in aerial and root tissues (mean $\log_2$(TPM+1) over the 5 ECT3-HT control samples) of the genes that are identified as targets only in aerial tissues or only in roots.

Figure supplement 1. Identification of ECT3 targets using HyperTRIBE (extended data).

Figure supplement 2. Characteristics of ECT3-HyperTRIBE editing sites relative to target expression levels.

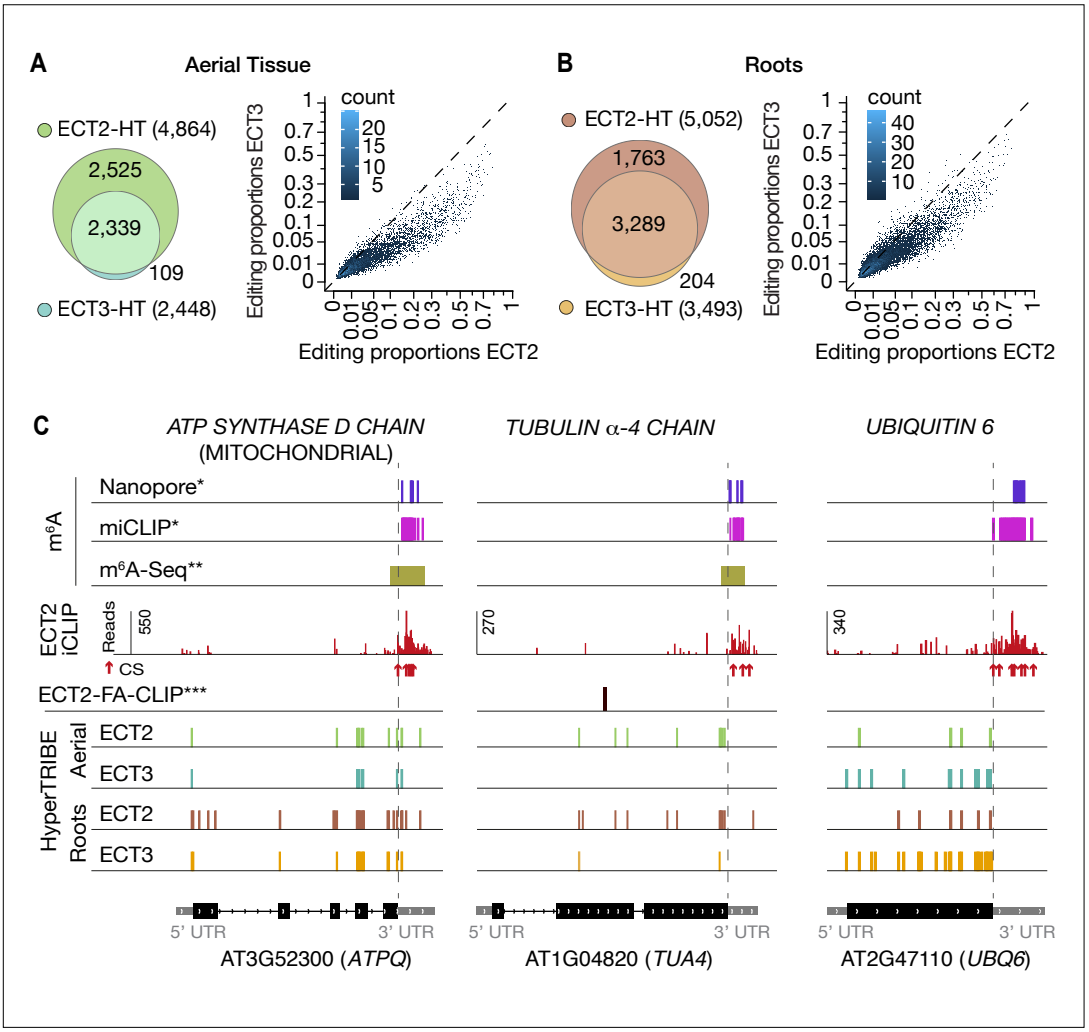

Figure 2. ECT3 targets are fewer and largely contained within ECT2 targets. (A, B) Left panels: overlap of ECT2-HT and ECT3-HT targets, for the set of commonly expressed genes, in aerial (A) and root (B) tissues. Right panels: Scatter plots showing the editing proportions of editing sites between ECT2-HT and ECT3-HT, for all significant positions common to both sets, separately for aerial tissues (A) and roots (B). **(C)** Examples of common ECT2 and ECT3 targets showing the distribution of ECT2/3-HT editing sites sites in either roots or shoots along the transcript. The distribution of ECT2-iCLIP reads and peaks, FA-CLIP peaks***, and m^{6}A sites*,** is also shown. * Parker et al. (2020); ** Shen et al. (2016); *** Wei et al. (2018).

Figure supplement 1. Sequencing depth of ECT2 and ECT3 HyperTRIBE RNA-seq data.

Figure supplement 2. ECT2 and ECT3 target each other and themselves.

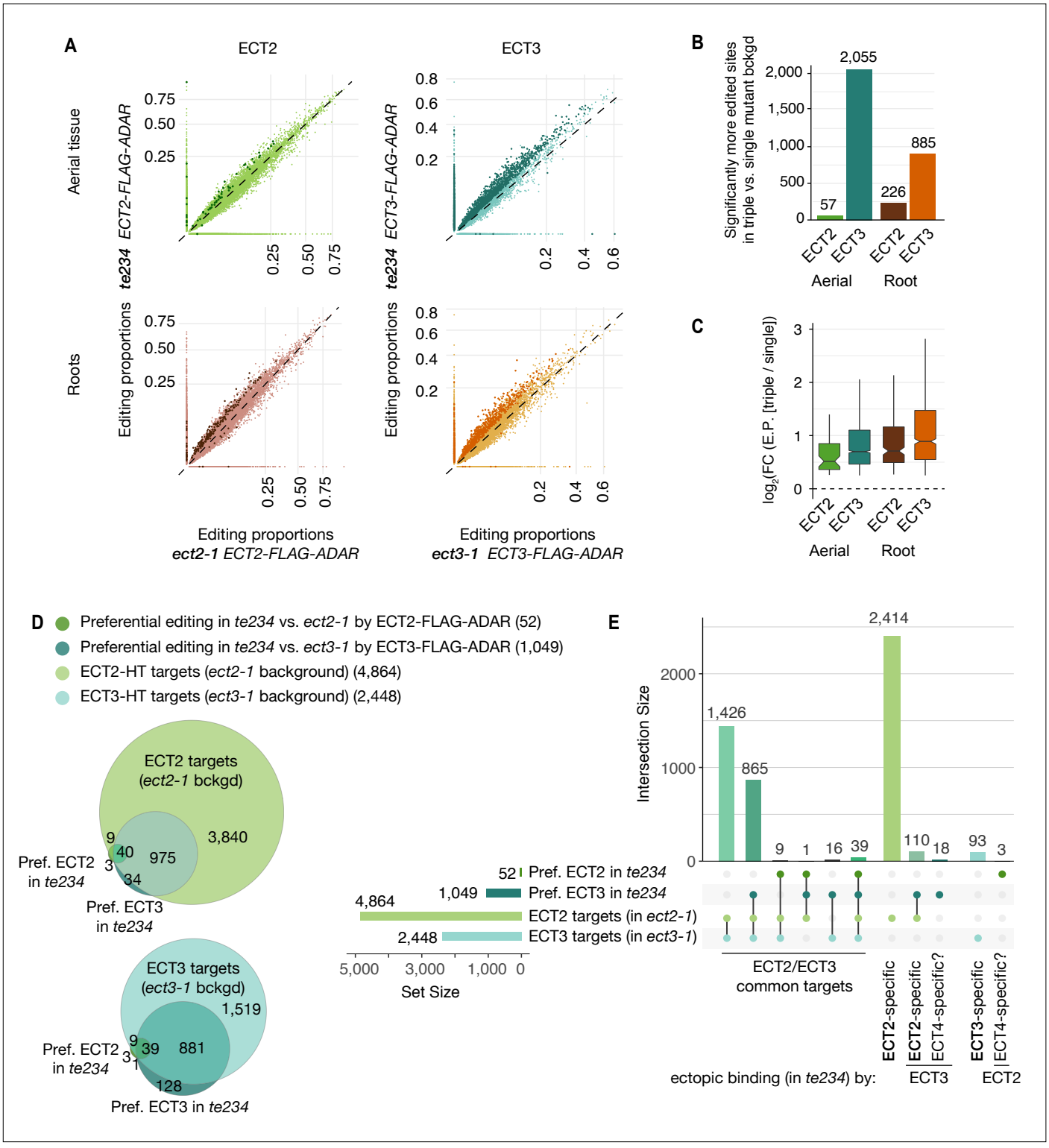

Figure 3. Redundancy between ECT2 and ECT3. (A) Scatterplots comparing the editing proportions of ECT2- and ECT3-FLAG-ADAR observed in triple vs. single mutant backgrounds in aerial and root tissues. They include all positions significantly edited with respect to FLAG-ADAR controls (p-value < 0.01, $\log_2$(FC)>1) in either background, with dots on the axes reflecting positions not significantly edited in one of the two backgrounds. Dots in darker shades indicate positions more highly edited in one background compared to the other (p-value < 0.1, log2(FC)>0.25 or log2(FC)<-0.25). **(B)** Barplots showing the number of positions significantly more edited in triple vs. single mutant background for each tissue and ECT protein. Positions significantly less edited in triple mutant background were less than 12 in all cases. **(C)** Boxplots showing fold changes in editing proportions between triple and single mutant background for the 2 ECT proteins and tissues studied. **(D,E)** Venn diagrams (D) and Upset plot (E) showing the overlap between the ECT2 and ECT3-HT target sets (in single mutant backgrounds) with the groups of genes with more highly edited positions in the triple mutant background in aerial tissues (the equivalent for roots is shown in *Figure3—figure supplement 2*).

Figure supplement 1. Expression levels (TPM) of the FLAG-ADAR-containing transgenes in all HyperTRIBE lines.

Figure supplement 2. Overlap between ECT2/3-HT targets in single and triple mutant background in roots.

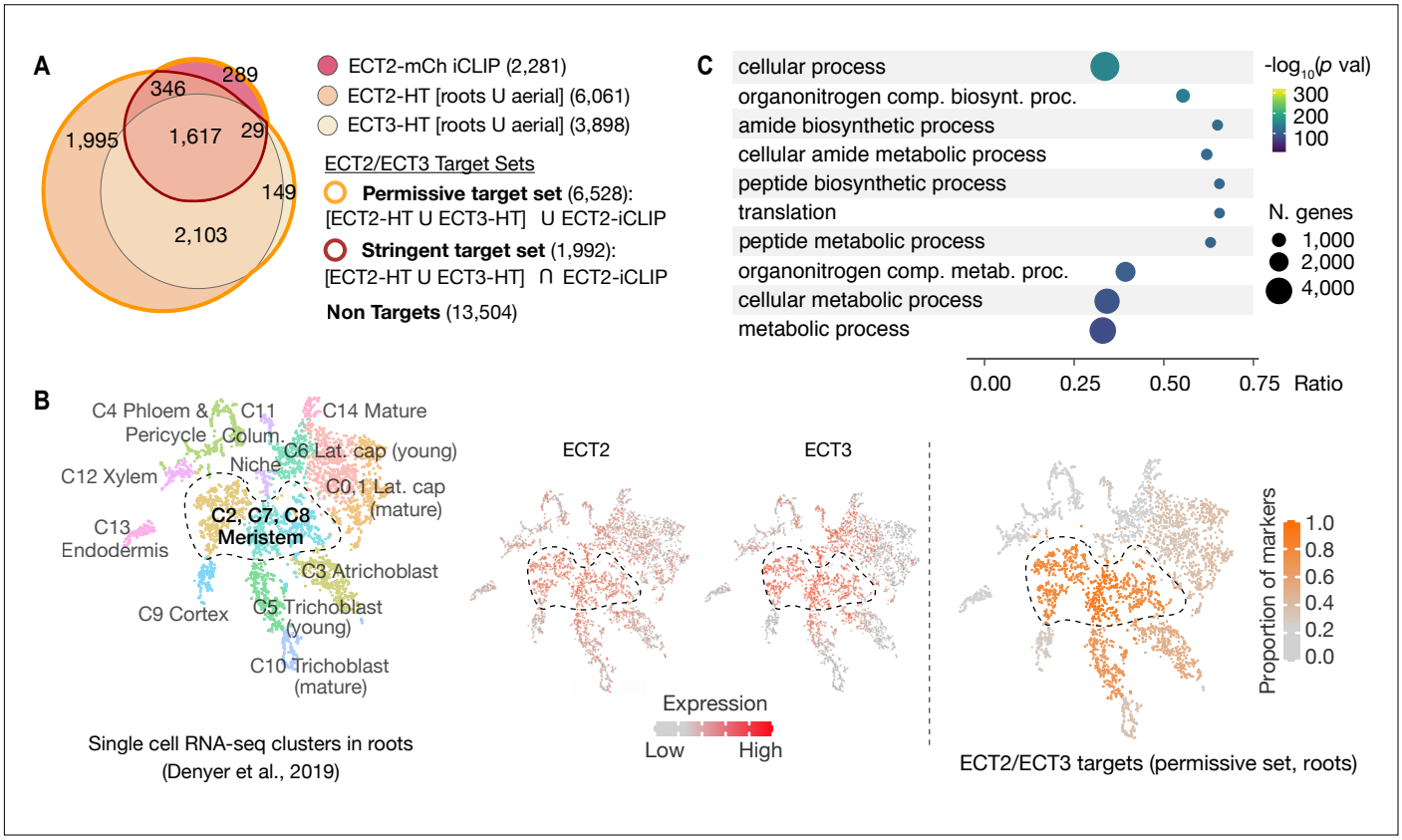

Figure 4. ECT2 and ECT3 targets are co-expressed with ECT2 and 3 in proliferating cells and enriched in biosynthetic processes. (A) Overlap between ECT2-iCLIP target genes with ECT2-HT and ECT3-HT target gene sets. Regions outlined in bold orange and red indicate the defined permissive and stringent ECT2/3 target sets in whole seedlings, respectively (aerial and root-specific target sets are shown in the figure supplement 1). Non-targets are all expressed genes (with detectable transcript levels in the corresponding HyperTRIBE RNA-Seq datasets) that are not in the permissive target set. **(B)** Left: t-SNE plot for scRNA-seq data in roots from Denyer et al. (2019), with cells colored according to their cell-type cluster definitions (see figure supplement 2 for details). Center: ECT2 and ECT3 single cell expression levels overlayed on to the t-SNE plot (Ma et al., 2020). Right: t-SNE plot with cell-type clusters shaded according to the proportion of marker genes from Denyer et al. (2019) that are targets of ECT2 or ECT3 in roots. Dashed enclosed region indicates clusters that contain meristematic cells. **(C)** The 10 most significantly enriched GO terms among ECT2/3 targets (permissive set).

Figure supplement 1. ECT2 and ECT3 target sets in aerial and root tissues.

Figure supplement 2. ECT2/ECT3 targets are co-expressed with *ECT2/3* in highly dividing root cells

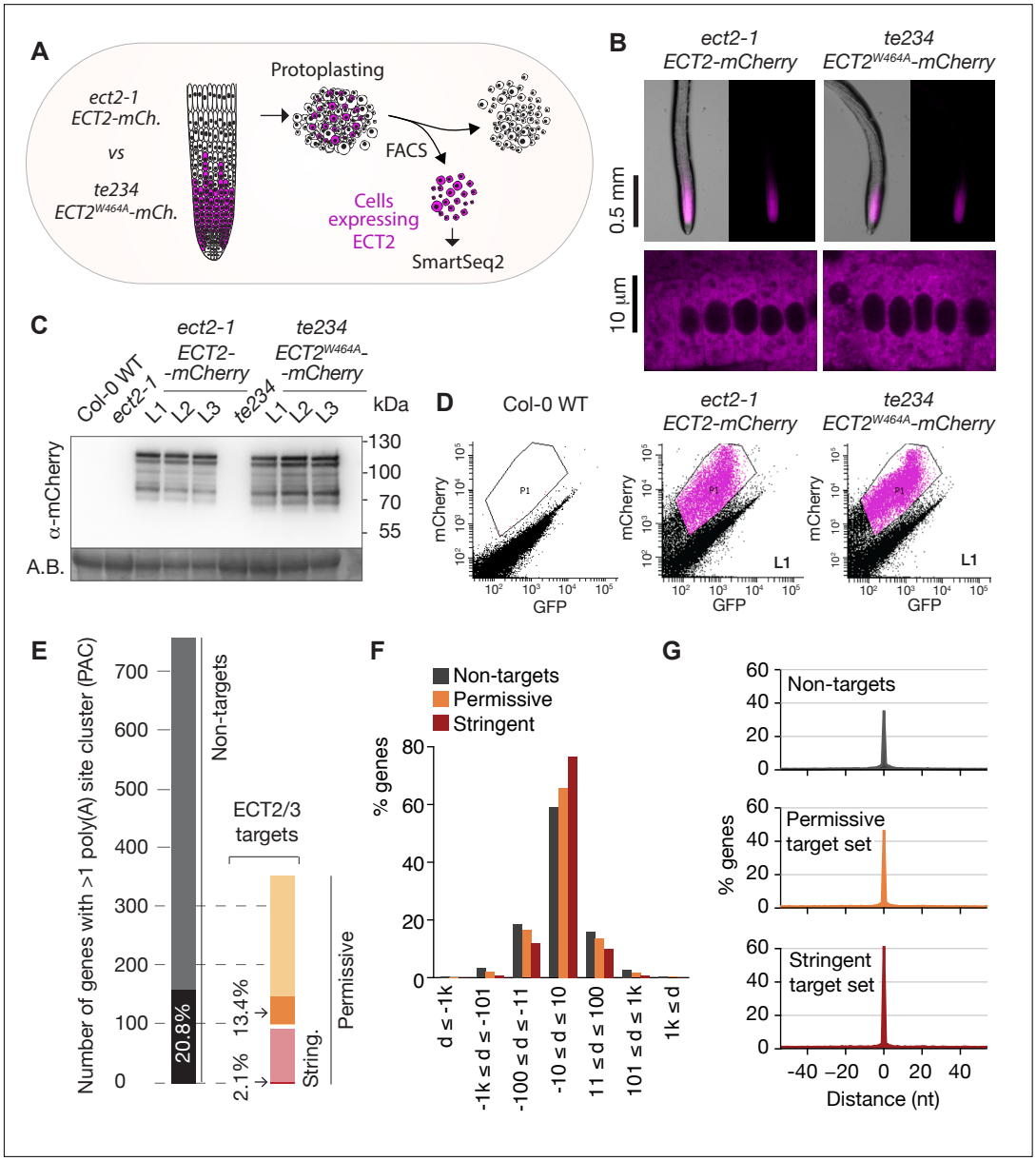

Figure 5. Poly(A) sites in ECT2/3 targets do not change upon loss of ECT2/3/4 function. (A) Experimental design. The experiment was performed once, using 3 biological replicates (independent lines) per group (genotype). **(B)** Expression pattern of ECT2-mCherry in root tips of *ect2-1 ECT2-mCherry* and *te234 ECT2^{W464A}-mCherry* genotypes by fluorescence microscopy. **(C)** Protein blot showing expression levels of ECT2-mCherry in the 3+3 lines of *ect2-1 ECT2-mCherry* and *te234 ECT2^{W464A}-mCherry* used as biological replicates for FACS selection of ECT2-expressing cells. Amido black (A.B.) is used as loading control. **(D)** Fluorescence profile (mCherry vs. GFP fluorescence) of root cells (protoplasts) from the transgenic lines in C. The complete set of lines/samples is shown in the figure supplement 1. Non-transgenic Col-0 WT is shown as control for background autofluorescence. Cells with a fluorescence profile within the outlined areas were selected for RNA extraction, Smart-seq2 library construction and sequencing. **(E)** Genes with more than one polyA site cluster (PAC) in the different target/non-target sets. Dark shades are genes in which the dominant PAC in *te234 ECT2^{W464A}-mCherry* samples differs from the one in *ect2-1 ECT2-mCherry*. **(F,G)** Distribution of distances (d [nt]) of the most common poly(A) site between *te234 ECT2^{W464A}-mCherry* and *ect2-1 ECT2-mCherry* samples for all genes where the most common poly(A) site could be determined in both genotypes (6,648 non-targets, 4,072 permissive targets, and 1,486 stringent targets). Negative values are upstream (5') and positive values are downstream (3') relative to the gene orientation. (F) Distances are binned by ±10, ±100, ±1000, and >1,000bp. (G) Distances are plotted by nucleotide in a ±40bp window.

Source data 1-3. Uncropped labelled panels and raw image files - *Figure 5C*.

Figure supplement 1. FACS-sorting of root protoplasts expressing ECT2-mCherry.

Figure supplement 2. Poly(A) sites do not change in ECT2/3 targets upon loss of ECT2/3/4 function (extended data).

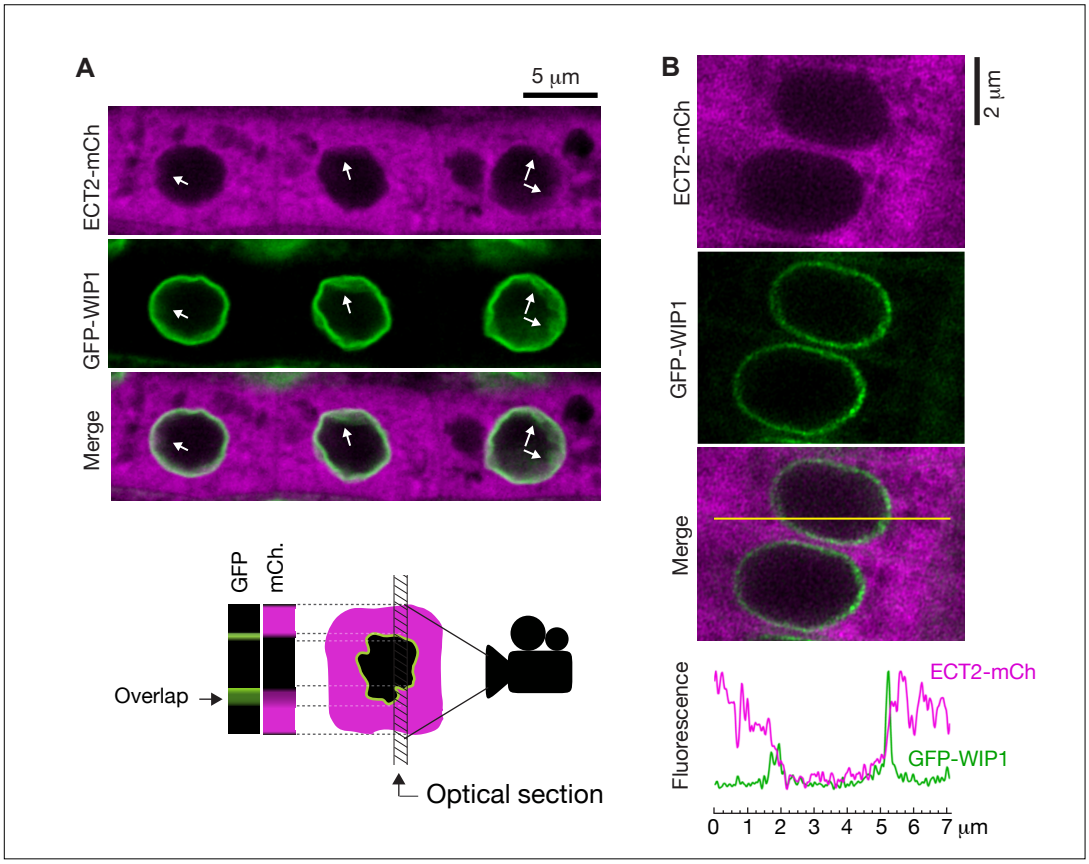

Figure 6. ECT2 is not in the nucleus. (**A**) Standard confocal microscopy of root cells co-expressing *ECT2-mCherry* and *GFP-WIP1*. White arrows indicate areas in which apparent spills of ECT2-mCherry signal into the nucleus overlap with blurry GFP signal from the nuclear envelope, a sign of not-perpendicularity between the envelope and the optical plane as exemplified on the cartoon at the bottom. (**B)** Airyscan super-resolution confocal microscopy of root cells as in A. The image is cropped from a larger picture shown in the figure supplement 1. mCherry and GFP fluorescence signals along the yellow line show absence of ECT2-mCherry inside the limits of the GFP-labelled nuclear envelope.

Figure supplement 1. Super-resolution confocal microscopy of cells co-expressing ECT2-mCherry and the nuclear envelope marker GFP-WIP1.

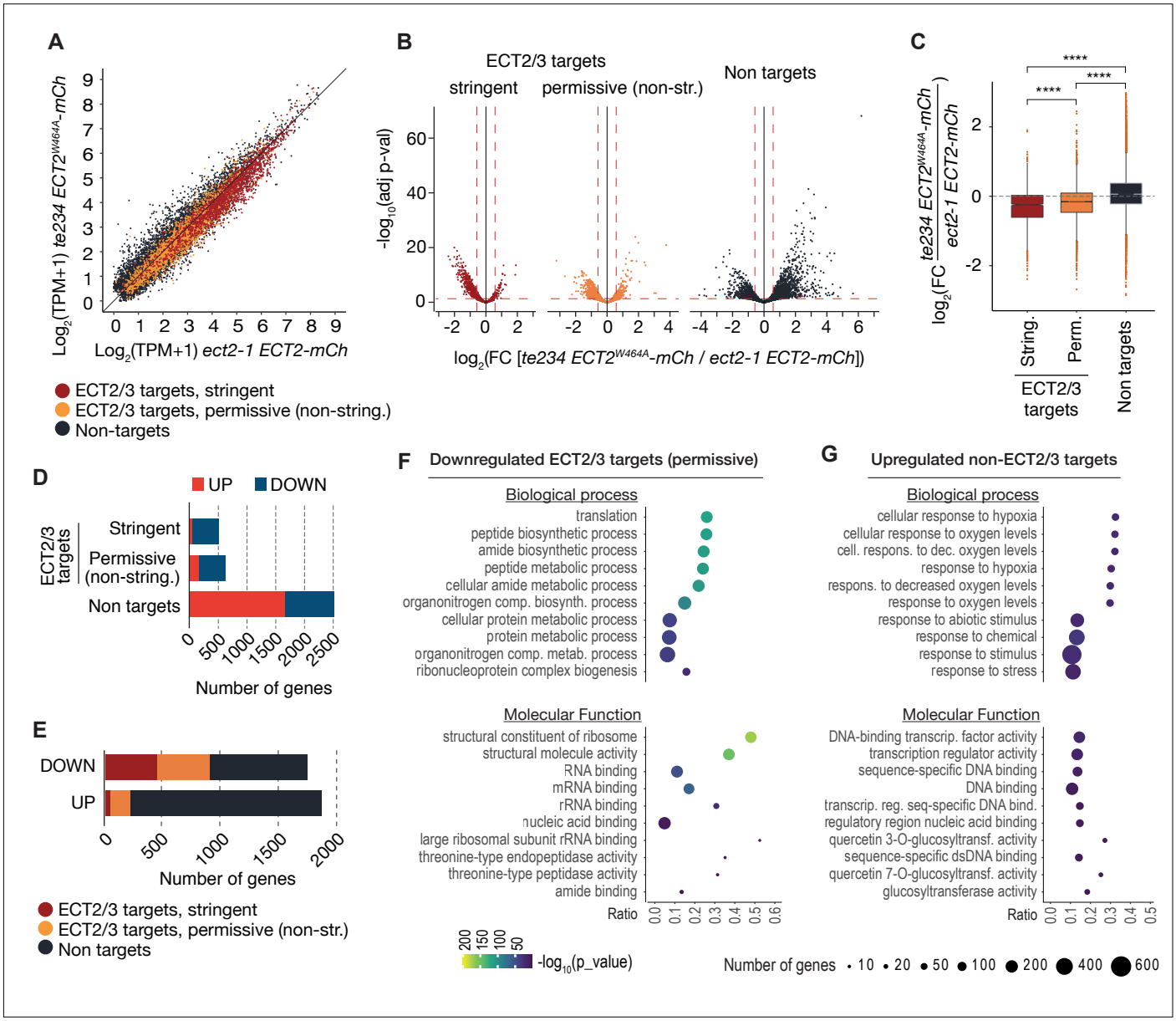

Figure 7. ECT2/3 targets are generally less abundant in cells without ECT2/3/4 function. (A) Scatterplot of TPM expression values in Smart-seq2 libraries of root protoplasts expressing ECT2-mCherry in *te234/ECT2^{W464A}-mCherry* vs. *ect2-1/ECT2-mCh* samples. **(B)** Volcano plots reveal genes differentially expressed between the genotypes described in A. **(C)** Boxplots of $\log_2$ fold change expression values between *te234/ECT2^{W464A}-mCherry* and *ect2-1/ECT2-mCh samples*. **(D,E)** Bar plots showing the amount of significantly up- and downregulated genes in ECT2/3 targets and non-targets. **(F,G)** List with the 10 most significantly enriched GO terms among significantly upregulated ECT2/3 targets (permissive set) (F), or downregulated non-targets (G) upon loss of ECT2/3/4 function.

Figure supplement 1. ECT2/3 targets are generally less abundant in root tips of *ect2/ect3/ect4* knockout plants.

A

AGI	Gene	FC	*p*-adj	ECT2/3 target
AT3G05690	NF-YA2	2.3	3.2e-06	permissive
AT1G72830	NF-YA3	1.6	0.0106	non-target
AT3G14020	NF-YA6	1.8	0.0012	non-target
AT1G17590	NF-YA8	1.6	0.0103	non-target
AT5G06510	NF-YA10	1.6	0.0216	non-target

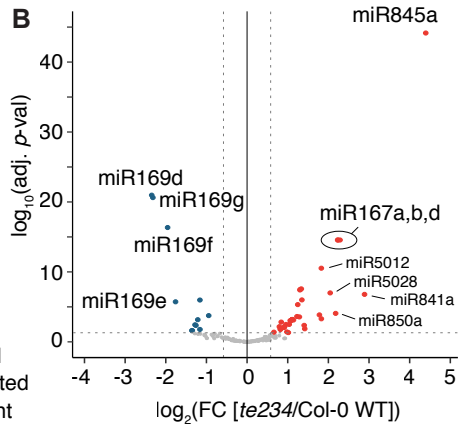

Figure 8. miRNA profile in root tips of *ect2/ect3/ect4* knockout plants. (A) Differential expression analysis of *te234* vs. Col-0 WT in 4-day-old root tips shows that expression of several stress-related NF-YA transcription factors (miR169defg targets) is induced in *te234* plants. FC, Fold Change [*te234*/WT]. **(B)** Volcano plot showing miRNAs differentially expressed in *te234* vs. Col-0 WT in 4-day-old root tips.

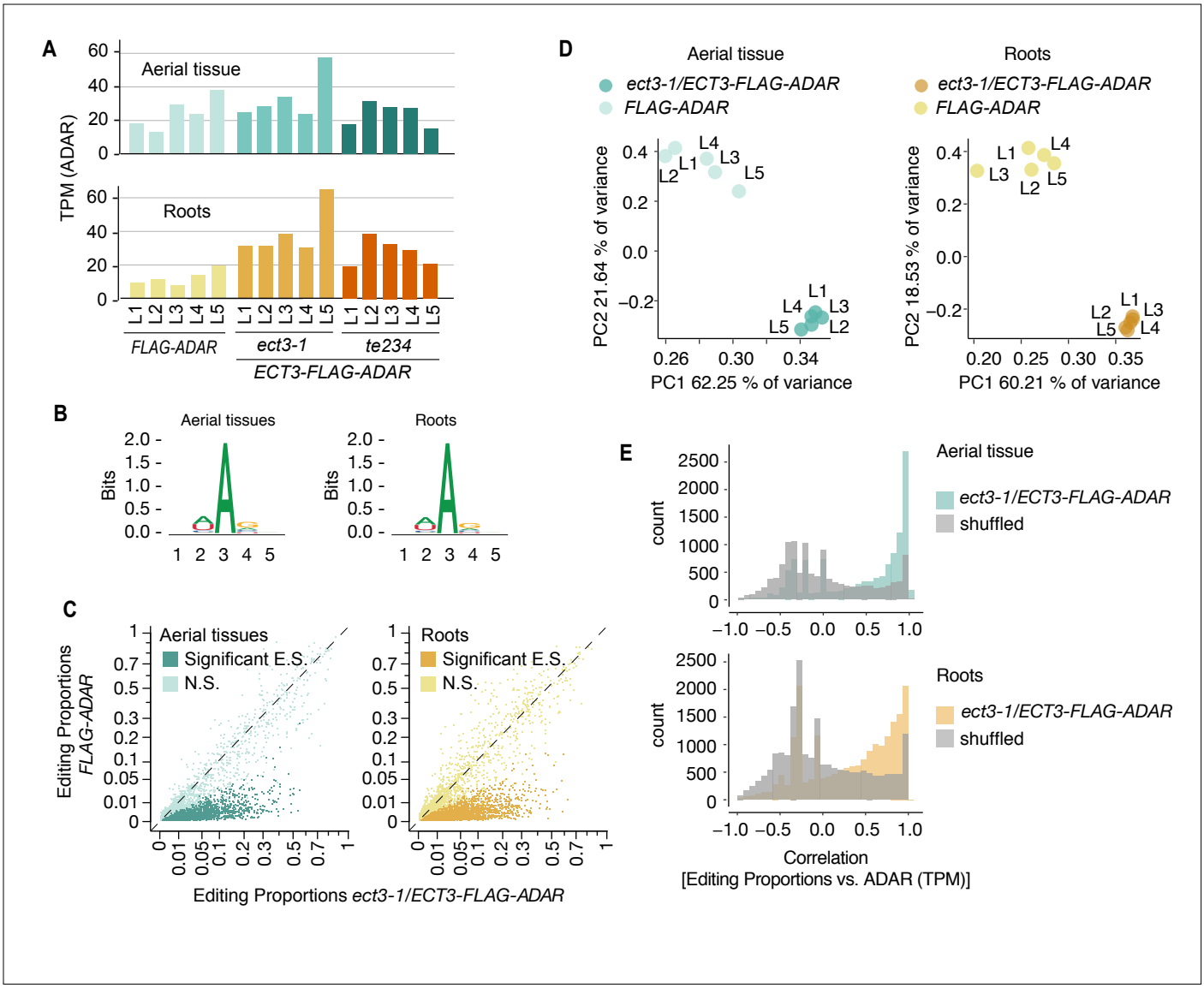

Figure 1—figure supplement 1. Identification of ECT3 targets using HyperTRIBE (extended data). **(A)** Expression levels of *ECT3-FLAG-ADAR* or *FLAG-ADAR* in apices (aerial tissues) or root tips of 10-day-old seedlings of the 5+5 independent transgenic lines (L1-L5) used for the experiment. **(B)** Consensus motif identified at significant editing sites of *ect3-1/ ECT3-FLAG-ADAR* lines. **(C)** Scatterplot of the editing proportions (E.P. = G/(A+G)) of potential and significant editing sites (E.S.) of *ect3-1/ECT3-FLAG-ADAR* lines compared to the *FLAG-ADAR* controls. N.S., not significant. **(D)** Principal component analysis of editing proportions at significant editing sites in ECT3-HT. **(E)** Distribution of the correlations between editing proportions and ADAR expression (TPM) for significant editing sites in *ect3-1/ECT3-FLAG-ADAR* lines. Background correlations are based on randomly shuffling ADAR expression for each site.

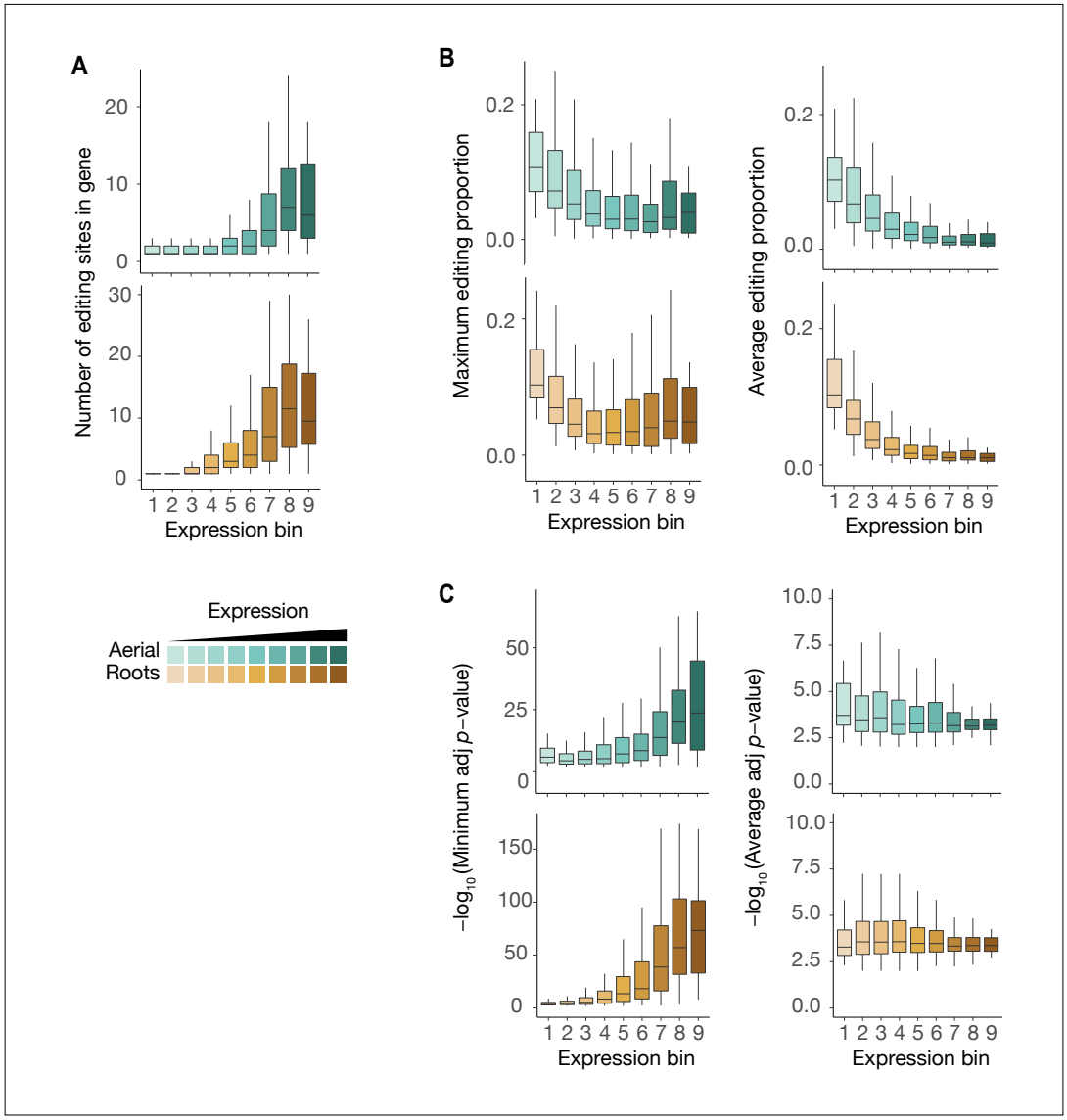

Figure 1—figure supplement 2. Characteristics of ECT3-HyperTRIBE editing sites relative to target expression levels. (A-C) Number of significant editing sites (A), maximum or average editing proportions (B), and significance of editing sites according to either minimum or average -$\log_{10}$(adjusted *p*-value) per gene (C) in ECT3-HT targets split according to their expression levels (mean $\log_2$(TPM+1) over the five ECT3-HT control samples)), in both aerial and root rissues.

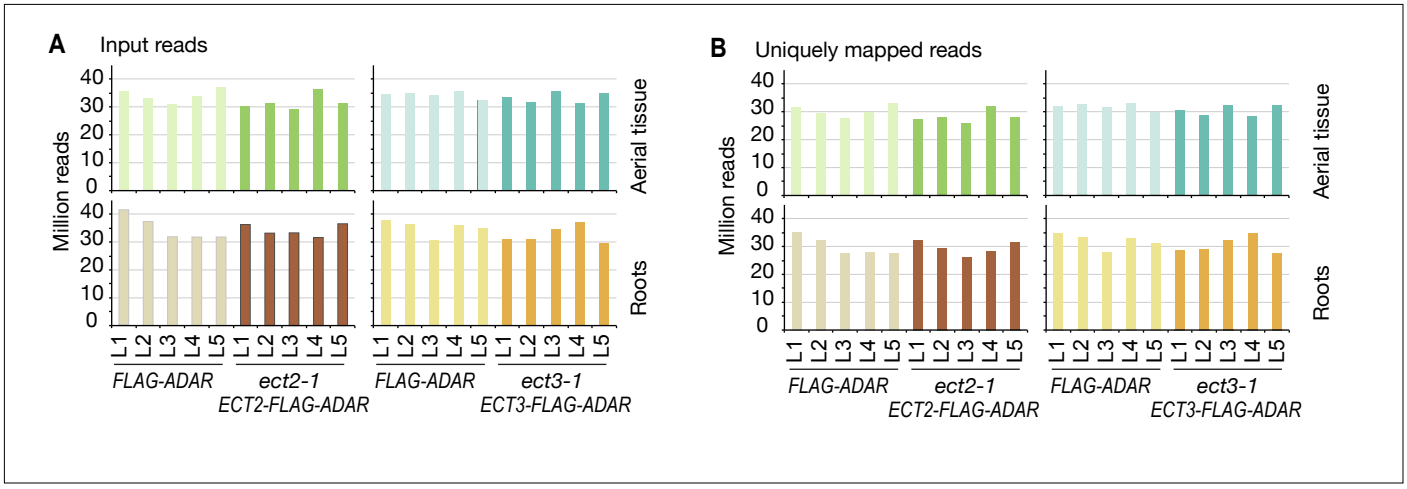

Figure 2—figure supplement 1. Sequencing depth of ECT2 and ECT3 HyperTRIBE RNA-seq data. (A,B) Number of input reads (A) and uniquely mapped reads (B) for ECT2-HT and ECT3-HT RNA-seq samples.

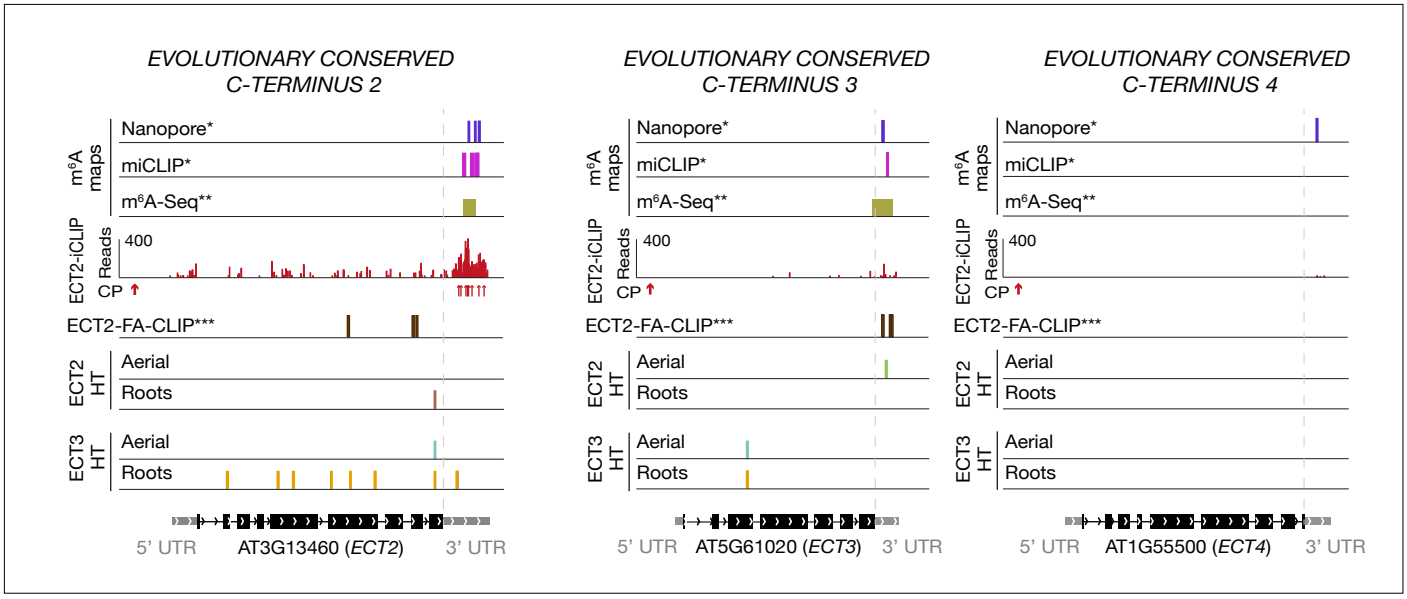

Figure 2—figure supplement 2. ECT2 and ECT3 target each other and themselves. Distribution of ECT2/3-HT editing sites and ECT2-iCLIP peaks along *ECT2/3/4*-encoding transcripts. *ECT2* is a target of ECT3, particularly clearly in roots, and *ECT3* is a target of ECT2 according to ECT2-HT in aerial tissues (not confirmed by ECT2-iCLIP). Although self-targeting of *ECT2* and *ECT3* may also be taken into consideration, it is important to notice that these targeted transcripts originate from transgenes. *ECT4* (right panel) does not appear as ECT2/3 target, but its low expression levels might account for a false negative. FA-CLIP peaks***, and m^{6}A sites*,** are shown as a reference. * Parker et al. (2020); ** Shen et al. (2016); *** Wei et al. (2018)

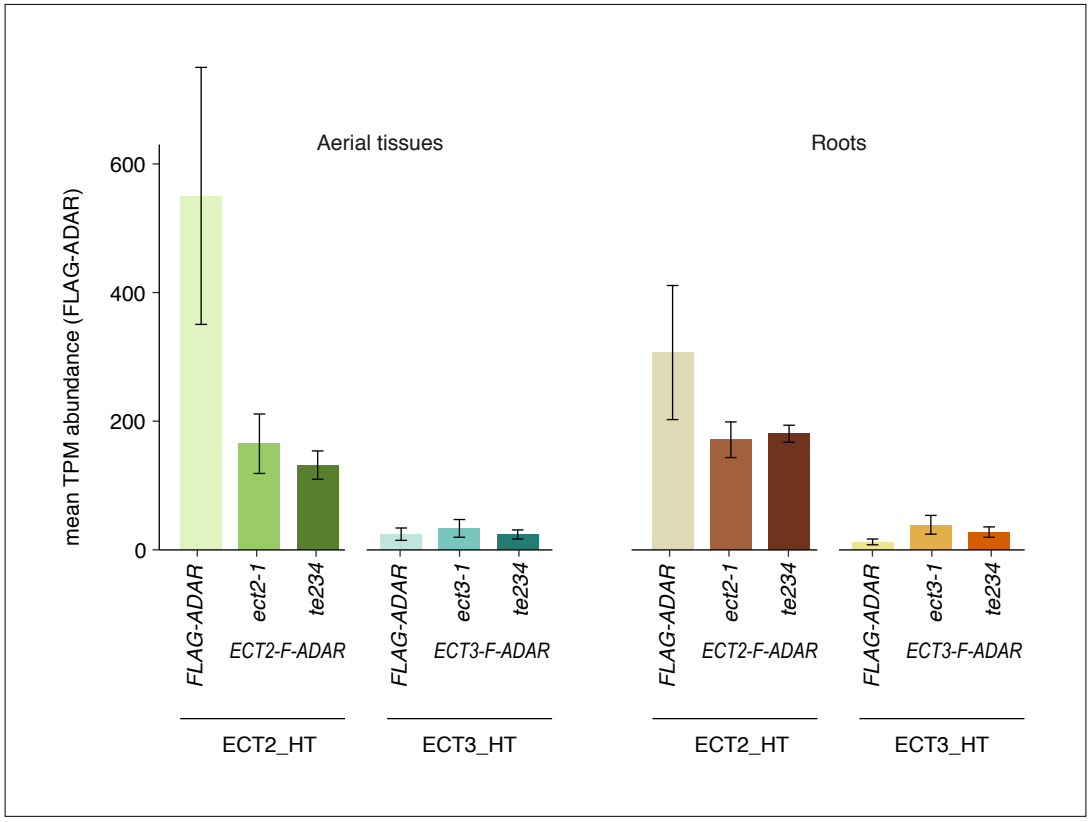

Figure 3—figure supplement 1. Expression levels (TPM) of the FLAG-ADAR-containing transgenes in all HyperTRIBE lines. TPMs for the five lines of every type have are averaged for simplicity. Notice that expression of ECT2/3-FLAG-ADAR transgenes is highly comparable in triple and single mutant backgrounds, ruling out the possibility of higher editing proportions in the triple mutant background due to higher abundance of the transgene. The expression of ECT3-FLAG-ADAR is generally lower than that of ECT2-FLAG-ADAR, as expected from the relative abundance of the endogenous transcrips (Arribas-Hernández et al., 2018).

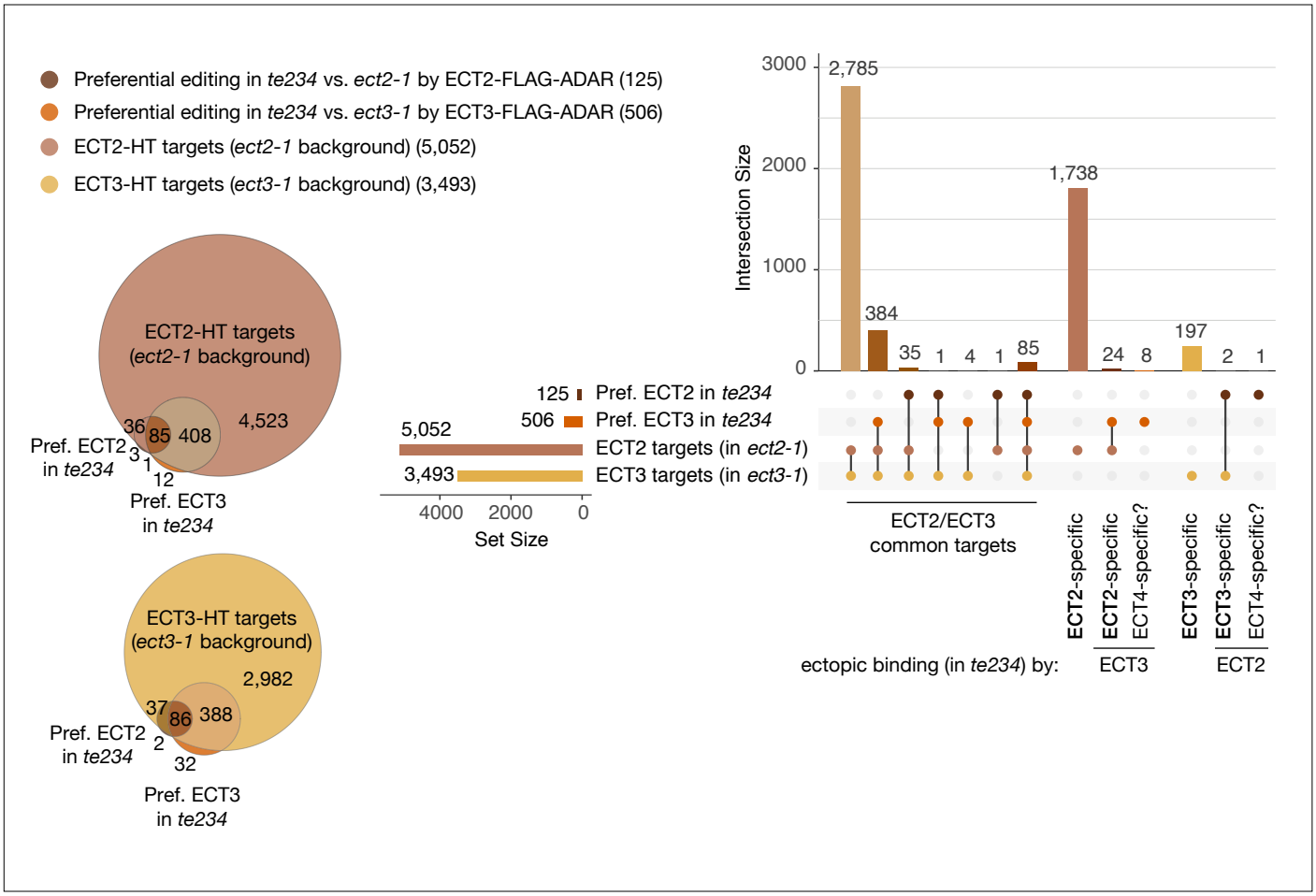

Figure 3—figure supplement 2. Overlap between ECT2/3-HT targets in single and triple mutant background in roots. Venn diagrams (left) and Upset plot (right) showing the overlap between the ECT2 and ECT3-HT target sets (in single mutant backgrounds) with the groups of genes with more highly edited positions in the triple mutant background in roots (the equivalent for aerial tissues is shown in *Figure 3D,E*).

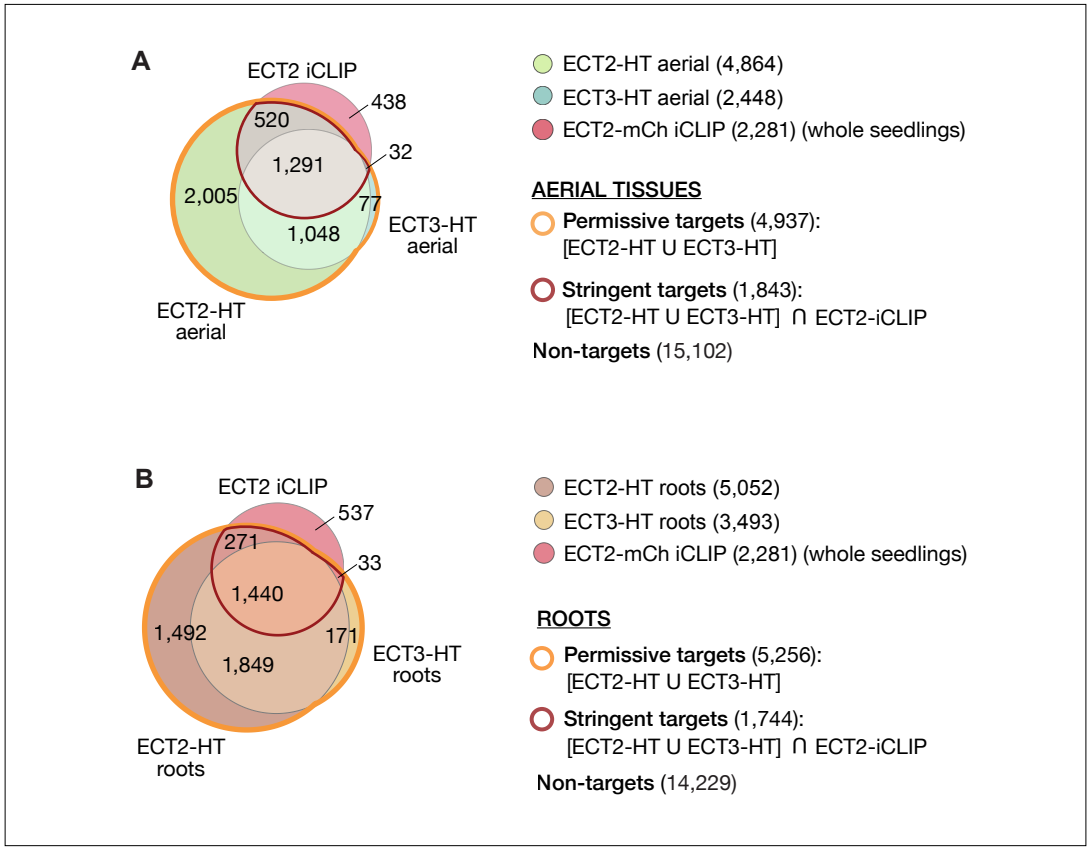

Figure 4—figure supplement 1. ECT2 and ECT3 target sets in aerial and root tissues. (A,B) Overlap between HyperTRIBE target sets of ECT2 and ECT3 in aerial tissue (A) or roots (B), and ECT2-iCLIP (whole seedlings). Genes contained within the outlined sets in roots constitute the permissive (orange outline) and stringent (dark red outline) ECT2/3 target sets (Supplementary File 4) for the subsequent transcriptome analyses of sorted root protoplasts. Non-targets are all genes with detectable transcript levels in the ECT2 or ECT3 (aerial or root) HT RNA-Seq datasets that are not in the permissive target set.

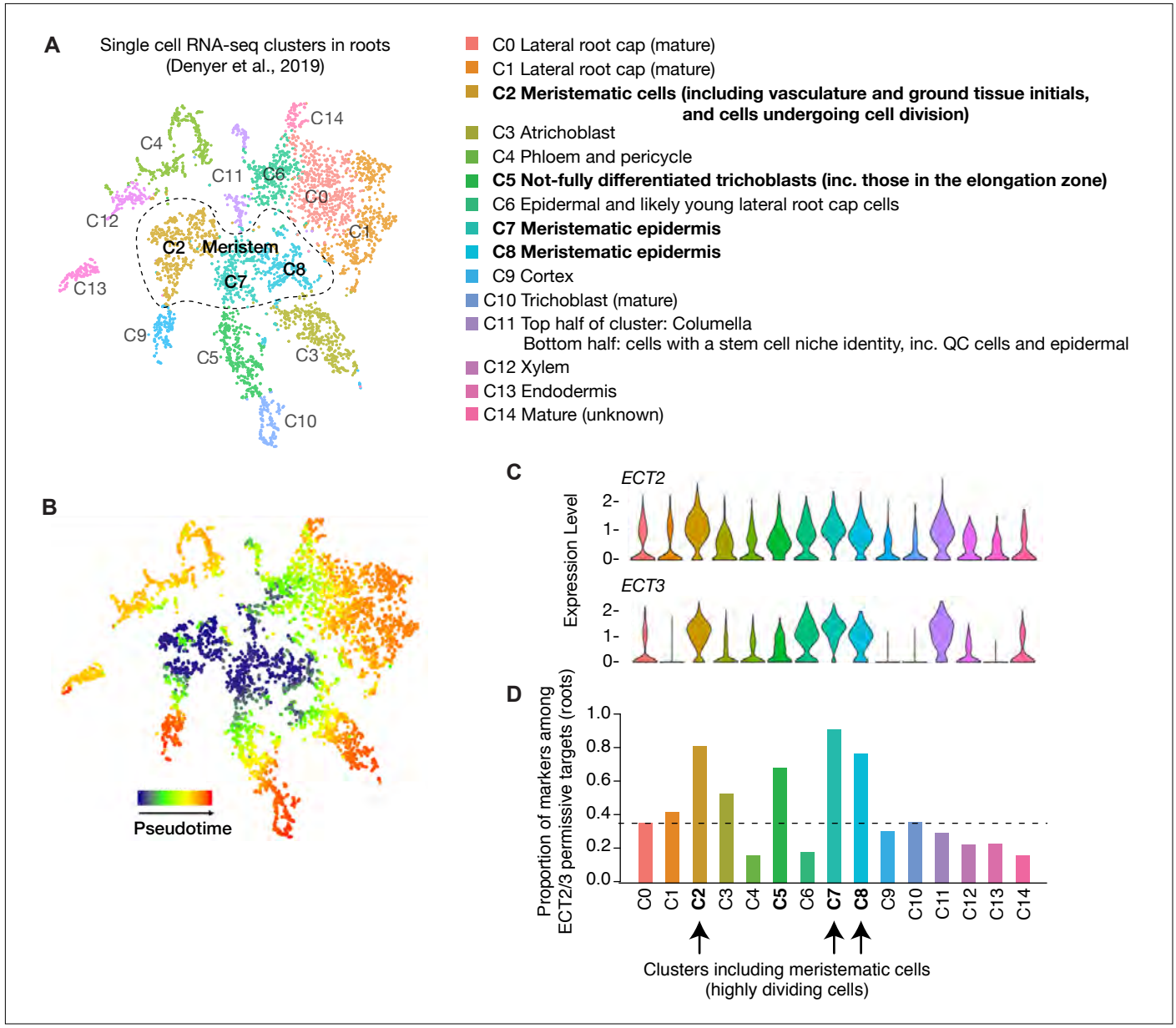

Figure 4—figure supplement 2. ECT2/ECT3 targets are co-expressed with *ECT2/3* in highly dividing root cells. (A) t-SNE plot for scRNA-seq data in roots from Denyer et al. (2019), with cells coloured according to their cell-type cluster definitions described on the right side (https://www.zmbp-resources.uni-tuebingen.de/timmermans/plant-single-cell-browser-arabidopsis-root-atlas/ and personal communication with Thomas Denyer). Dashed-enclosed region indicates clusters that contain meristematic cells. **(B)** Temporal reference map derived from pseudotime analysis of cells (Denyer et al., 2019) illustrates the progressive maturation of cells from the meristem core (reproduced with permission from Ma et al. (2020)). **(C)** Violin plot showing *ECT2* and *ECT3* single cell expression levels in the different clusters defined in A. These plots and their corresponding grey-red shaded t-SNE plots in *Figure 4B* (centre panels) were obtained from the above-mentioned website (Ma et al., 2020). **(D)** Box plot showing the proportion of marker genes from Denyer et al. (2019), which are targets of ECT2 or ECT3 in roots. These values were used to obtain the corresponding grey-orange shaded t-SNE plot shown in *Figure 4B* (right panel).

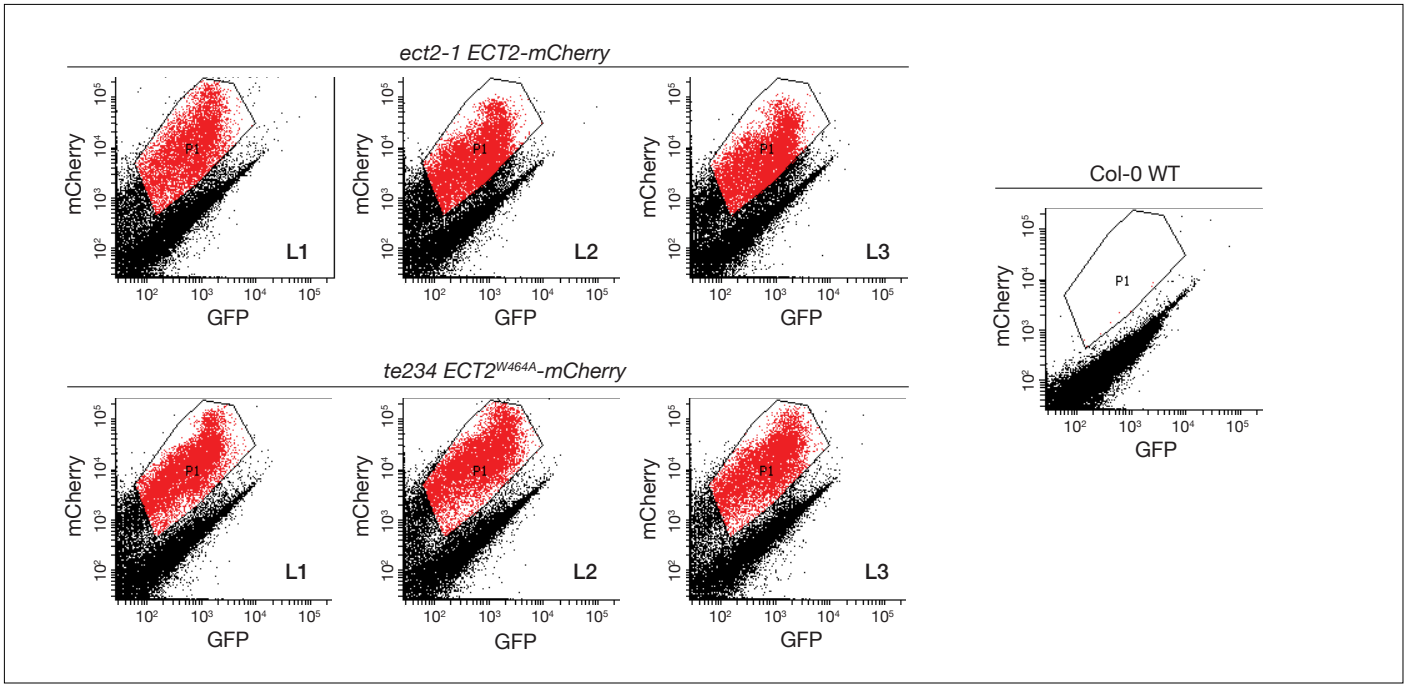

Figure 5—figure supplement 1. FACS-sorting of root protoplasts expressing ECT2-mCherry. Fluorescence profile (mCherry vs. GFP fluorescence) of root cells (protoplasts) from the transgenic lines used as replicates for transcriptomic analyses (*Figures 5, 7*). Non-transgenic Col-0 WT is shown as control for background autofluorescence. Cells with a fluorescence profile within the outlined areas were selected for RNA extraction, Smart-seq2 library construction and sequencing.

A

Sample	Total reads	poly(A) reads	poly(A) %	Merged
*ect2-1 ECT2-mCh*_L1	36,694,656	617,249	1.7%	
*ect2-1 ECT2-mCh*_L2	16,698,183	288,965	1.7%	1,355,603
*ect2-1 ECT2-mCh*_L3	26,218,902	449,389	1.7%	
*te234 ECT2^{W464A}-mCh*_L1	28,983,562	557,920	1.9%	
*te234 ECT2^{W464A}-mCh*_L2	20,164,588	369,574	1.8%	1,263,560
*te234 ECT2^{W464A}-mCh*_L3	19,826,857	336,066	1.7%	

B

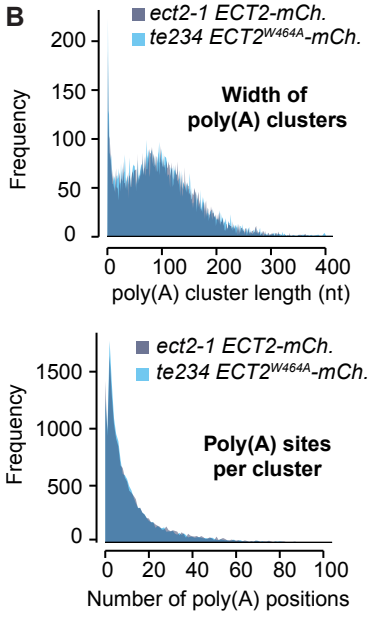

C

	Number of genes	Genes with PACs		Genes with > 1 PAC		Genes with different dominant PAC	
		Number	%	Number	%	Number	%
Stringent targets	1744	1492	85.6%	95	6.4%	2	2.1%
Permissive targets	5256	4230	80.5%	350	8.3%	47	13.4%
Non-targets	14229	7535	53.0%	764	10.1%	159	20.8%

D

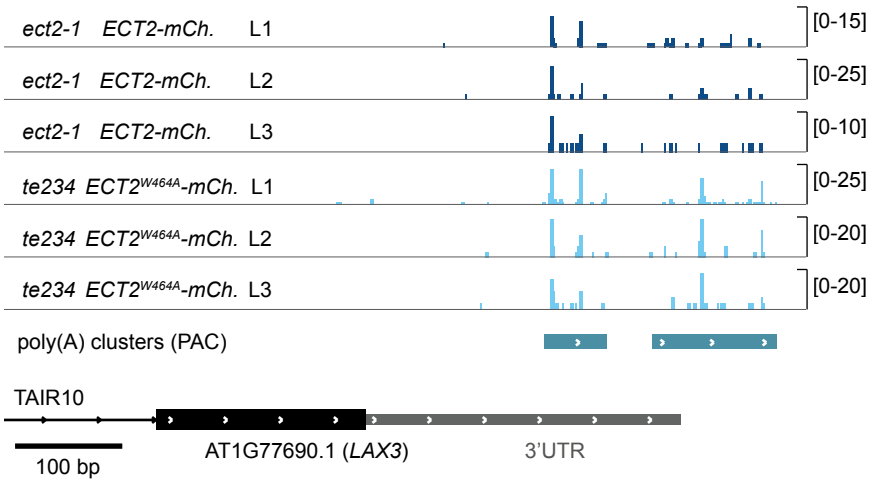

E

		n° genes	TPM
Stringent targets	All	1744	131
Non targets	All	14229	25
	More highly expressed	2200	132.7

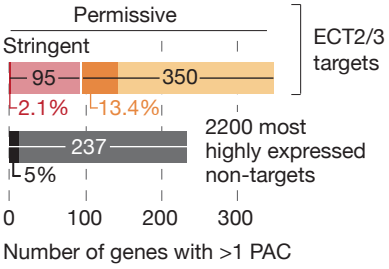

Figure 5—figure supplement 2. Poly(A) sites do not change in ECT2/3 targets upon loss of *ECT2/3/4* function (extended data). (A) Summary of poly(A)-containing reads (i.e. reads with at least 9 untemplated As) after removal of reads mapping upstream of purine-rich sites. These reads were used for cluster identification, yielding 17,028 putative poly(A) site clusters (PACs), from which 14,667 were retained after further filtering of potential false positives (see Methods). **(B)** Features of PACs. (Upper panel) Genomic distance between most upstream and most downstream poly(A) site within each cluster (median length of 105 bp). (Lower panel) Total number of genomic positions within the cluster where at least 1 read with an untemplated poly(A) tail was detected (median of 12 poly(A) sites per cluster). **(C)** PACs sorted by ECT2/3 target status. Percentages of genes with more than 1 PAC refer to the number of genes with PACs. Percentages of genes with a dominant PAC (defined as the cluster with the most reads) that is different between *te234 ECT2^{W464A}-mCherry* and *ect2-1 ECT2-mCh* samples refer to the number of genes with more than 1 PAC. **(D)** Variation in dominant polyadenylation sites for the non-ECT2/3-targeted transcript *LAX3*, an example of gene with different dominant PAC. Independently of the fact that the total amount of poly(A) reads is generally higher in *te234 ECT2^{W464A}-mCherry* compared to *ect2-1 ECT2-mCh* samples (notice that the scales have been adjusted for optimal comparison of PAC usage within samples), the ratio between the number of reads in the upstream and the downstream clusters is different in the 2 genotypes. Transcript annotation is based on TAIR10. **(E)** Mean TPMs (Smart-seq2 data of sorted protoplasts, combining all 6 samples) of genes in the different ECT2/3 targets groups (upper panel). The significantly lower likelihood for ECT2/3 targets to have a different dominant PAC upon loss of ECT2/3/4 function depletion compared to non targets (*Figure 5E*) could be due to differences in transcript abundance between the target and non-target groups. Looking at only the 2200 most highly expressed non-target genes, only 5.5% of these genes have a different dominant PAC in *te234 ECT2^{W464A}-mCherry* than *ect2-1 ECT2-mCh* samples (lower panel, dark shading refers to genes with different dominant PAC as in *Figure 5E*), significantly smaller than the percentage for all non-target genes (20.8%, *Figure 5E*) (p=3.2e-9, Fisher's exact test).

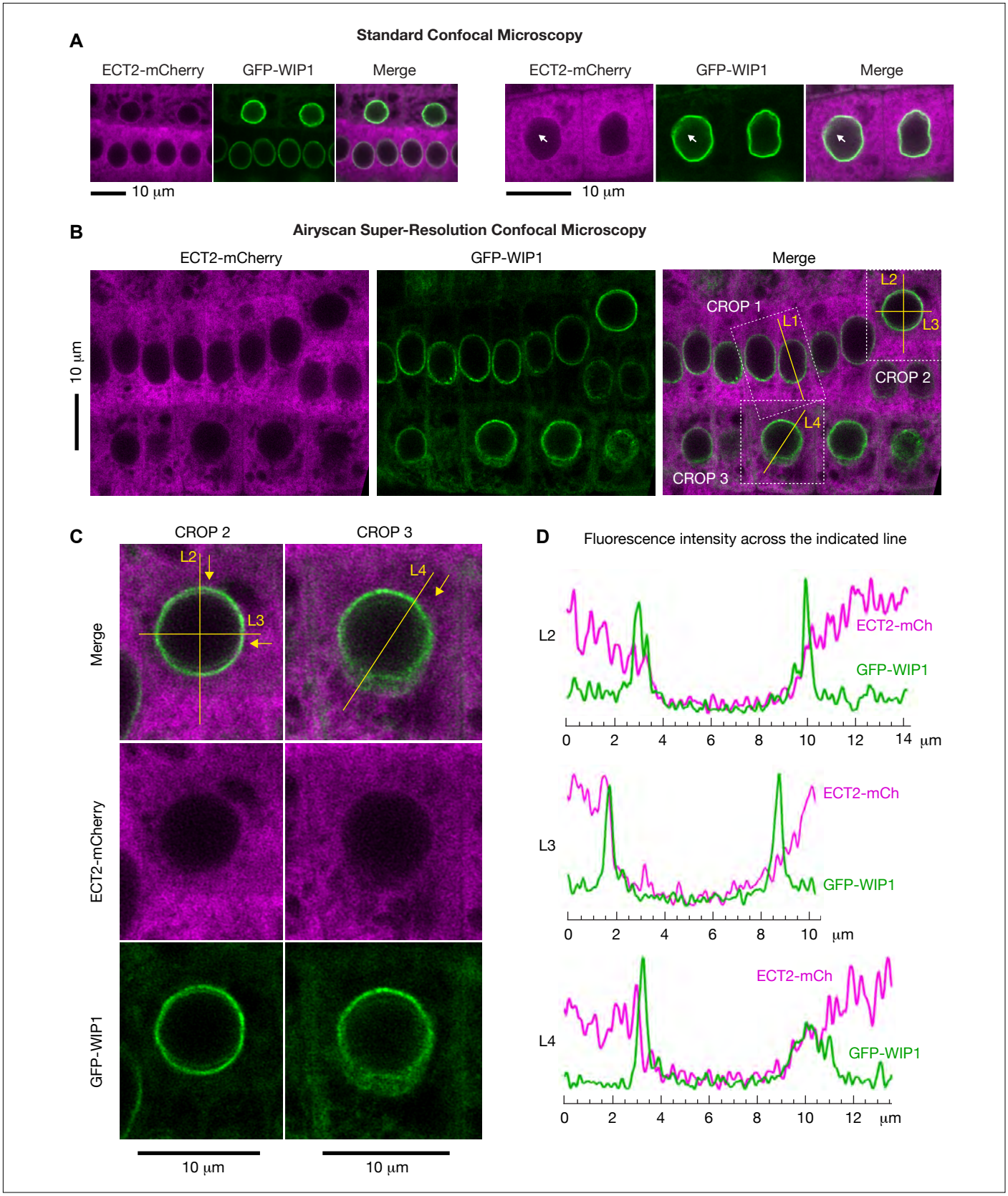

Figure 6—figure supplement 1. Super-resolution confocal microscopy of cells co-expressing ECT2-mCherry and the nuclear envelope marker GFP-WIP1. (A) Standard confocal microscopy of root cells co-expressing *ECT2-mCherry* and *GFP-WIP1* as in *Figure 6A*. **(B-D)** Airyscan super-resolution confocal microscopy of root cells as in A. White dashed outlines in (B) are magnified in (C) (crop 2 and 3), and mCherry/GFP fluorescence along the yellow lines (L2-4) is plotted in (D). Yellow arrows indicate the direction of the fluorescence plots from left to right. Magnification of crop 1 and fluorescence intensity along L1 is shown in *Figure 6B* .

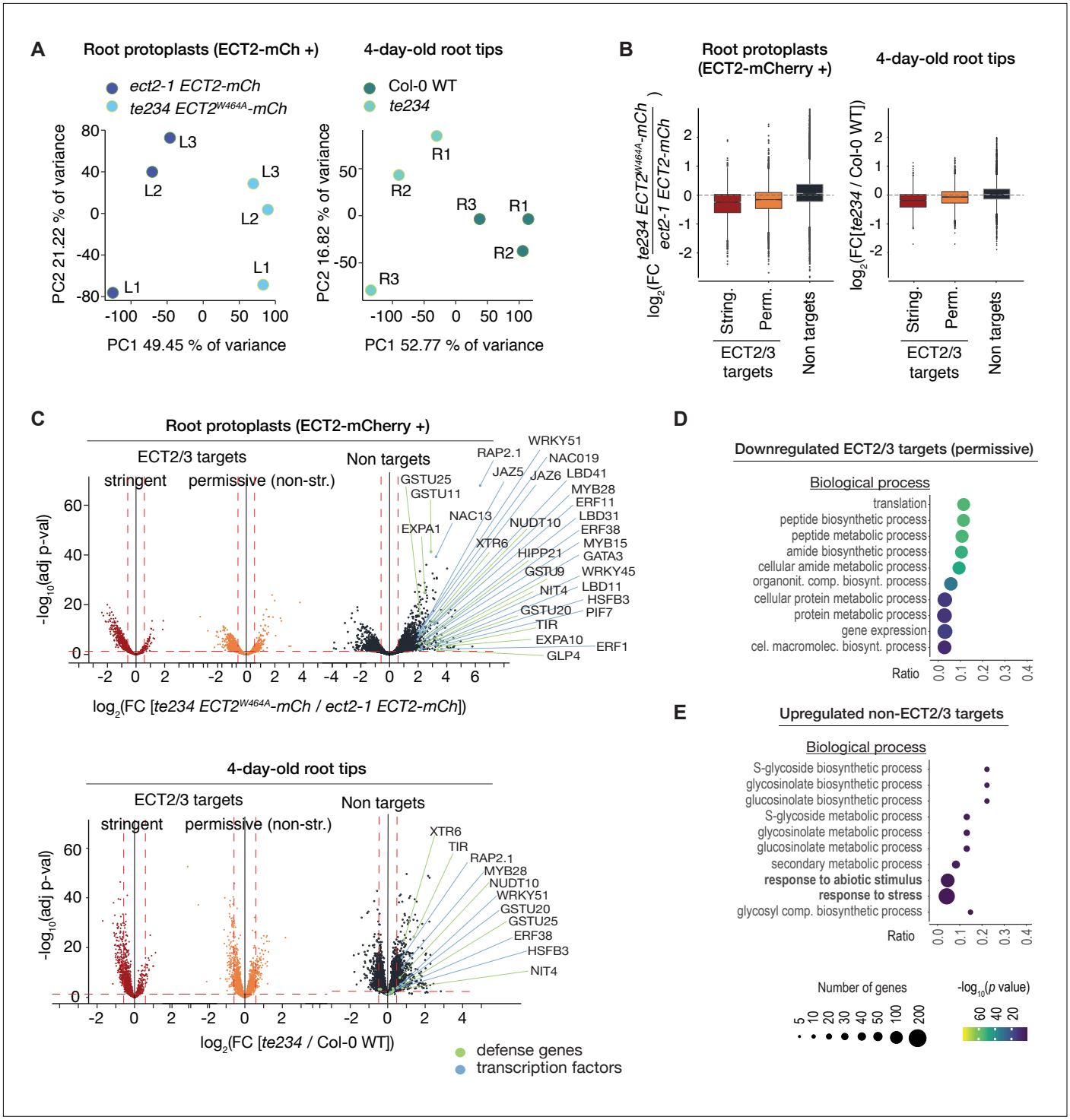

Figure 7—figure supplement 1. ECT2/3 targets are generally less abundant in root tips of *ect2/ect3/ect4* knockout plants. (A) Principal component analysis of transcriptome expression values (TPM) in Smart-seq2 libraries from FACS-sorted root protoplasts expressing *ECT2-mCherry* in *te234/ECT2^{W464A}-mCherry* and *ect2-1/ECT2-mCh* 5-day-old seedlings (left panel), or in RNA-seq libraries obtained from root tips of *te234* and wild type 4-day-old seedlings (right panel). **(B)** Boxplots of $\log_2$ fold change expression values between the genotype-pairs described in A. **(C)** Volcano plots showing genes differentially expressed between the genotype-pairs described in A. Upregulated non-ECT2/3 targeted transcription factors and stress-responsive genes are marked. **(D,E)** List with the 10 most significantly enriched GO terms among significantly upregulated ECT2/3 targets (permissive set) (D), or downregulated non-targets (E) in root tips of *ect2/3/4* knockout plants (*te234*) compared to wild type.